NASA Public Access
Author manuscript
Nature. Author manuscript; available in PMC 2019 May 16.

Published in final edited form as:
Nature. 2018 May ; 557(7707): 651–659. doi:10.1038/s41586-018-0123-1.

Emerging Trends in Global Freshwater Availability

M. Rodell[a], **J.S. Famiglietti**[b], **D.N. Wiese**[b], **J.T. Reager**[b], **H.K. Beaudoing**[a,c], **F.W. Landerer**[b], and **M.-H. Lo**[d]

[a]Hydrological Sciences Laboratory, NASA Goddard Space Flight Center, Greenbelt, Maryland, USA

[b]Jet Propulsion Laboratory, California Institute of Technology, Pasadena, California, USA

[c]Earth System Science Interdisciplinary Center, University of Maryland, College Park, Maryland, USA

[d]Department of Atmospheric Sciences, National Taiwan University, Taipei, Taiwan

Summary

Freshwater availability is changing worldwide. Here we quantify 34 trends in terrestrial water storage (TWS) observed by the Gravity Recovery and Climate Experiment (GRACE) satellites during 2002–2016 and categorize their drivers as natural interannual variability, unsustainable groundwater consumption, or climate change. Several of these trends had been lacking thorough investigation and attribution, including massive changes in northwestern China and the Okavango delta. Others are consistent with climate model predictions. This observation-based assessment of how the world's water landscape is responding to human impacts and climate variations provides a blueprint for evaluating and predicting emerging threats to water and food security.

Groundwater, soil moisture, surface waters, snow, and ice are dynamic components of the terrestrial water cycle[1, 2, 3]. They are not static on an annual basis (as early water budget analyses supposed), yet absent hydroclimatic shifts or significant anthropogenic stresses they typically remain range-bound. Recent studies have identified locations where terrestrial water storage (TWS; the sum of these five components) appears to be trending below previous ranges, notably where ice sheets or glaciers are diminishing in response to climate change[4, 5] and where groundwater is being withdrawn at an unsustainable rate[6, 7, 8].

Accurate accounting of changes in freshwater availability is essential for predicting regional food supplies, human and ecosystem health, energy generation, and social unrest. Groundwater is particularly difficult to monitor and manage because aquifers are vast and unseen, yet groundwater meets the domestic needs of roughly half of the world's population[9] and boosts food supply by providing for 38% of global consumptive irrigation

Reprints and permissions information are available at www.nature.com/reprints.

Corresponding Author Matthew Rodell, + 1 301-286-9143 Matthew.Rodell@nasa.gov.

Author Contributions

M.R. and J.S.F. performed background research and designed the study with input from J.T.R. and M.-H.L. D.N.W. and J.T.R. led the GRACE data and error analysis with assistance from F.W.L. M.R. and F.W.L. designed the figures with additional data prepared by H.K.B. M.R. and J.S.F. wrote the manuscript. All authors discussed the results and commented on the manuscript.

The authors claim no competing financial interests.

NASA Author Manuscript
NASA Author Manuscript
NASA Author Manuscript

NASA Author Manuscript NASA Author Manuscript NASA Author Manuscript

water usage[10]. Nearly two-thirds of terrestrial aquatic habitats are being increasingly threatened[11] while the precipitation and river discharge that support them are becoming more variable[12]. A recent study[11] estimates that almost 5 billion people live in areas where threats to water security are likely, a situation that will only be exacerbated by climate change, population growth, and human activities. The key environmental challenge of the 21st century then may well be one of globally-sustainable water resources management.

Much of our knowledge of past and current freshwater availability comes from a limited set of ground-based, point observations. Assessing changes in hydrologic conditions at the global scale is exceedingly difficult using in situ measurements alone, due to the cost of installing and maintaining instrument networks, gaps in those networks, and a lack of digitization and sharing of what data do exist[13]. Satellite remote sensing has proven crucial to monitoring water storage and fluxes in a changing world, enabling a truly global perspective that spans political boundaries[14]. In particular, since its launch in 2002, the GRACE mission[15] has tracked ice sheet and glacier ablation, groundwater depletion, and other TWS changes[16, 17, 18, 19]. On a monthly basis GRACE can resolve TWS changes with sufficient accuracy over scales that approximately range from 200,000 km^2 at low latitudes to 90,000 km^2 near the poles[1]. However, due to GRACE'S coarse spatial resolution, inability to partition component mass changes, and the brevity of the time series, proper attribution of the TWS changes requires comprehensive examination of all available auxiliary information and data, which has never before been performed at the global scale.

Here we map TWS change rates around the globe based on 14 years (April 2002 - March 2016) of GRACE observations (Figure 1). The GRACE data were processed using an advanced mass concentration[20] ("mascon") approach that enables improved signal resolution relative to the standard spherical harmonic technique[21]. Best fit linear rates of change after removing the seasonal cycle (referred to herein as "apparent trends") are presented in Table 1 for 34 study regions. For context, the largest man-made reservoir in the U.S., Lake Mead, has a capacity of about 32 Gt; during the study period all but one of the 34 regions lost or gained more water than that and eleven of them lost or gained more than ten times that amount. The reported uncertainty bounds are typically low because error in the removal of glacial isostatic adjustment (GIA) signals is the only major source of noise in the secular signal; low uncertainty does not, on its own, imply that the apparent trends existed before the GRACE period or will continue into the future. The coefficient of determination (r^2), representing the "goodness of fit" of the regressed linear trends, is included in Table 1 to quantify the strength of the apparent trends relative to non-secular interannual variability. It is hence a useful but by no means conclusive piece of evidence for predicting whether the trend will be fleeting or enduring, reflecting the cohesiveness of the TWS time series tendencies in Figures ED1-ED4. We attribute the trends to natural variability, direct human impacts, or climate change and forecast the likelihood that they will continue based on 1979–2016 precipitation data from the Global Precipitation Climatology Project version 2.3 (GPCP)[22] (see Figures ED5-ED8), an irrigated area map[23], satellite-based lake level altimetry time series[24], Landsat imagery, and published reports of human activities including agriculture, mining, reservoir operations, and inter-basin water transfers. Further, for each region we provide the median climate model prediction of precipitation changes between 1986–2005 and 2081–2100, under the Representative Concentration Pathways 8.5 W/m^2

NASA Author Manuscript NASA Author Manuscript NASA Author Manuscript

(RCP8.5; “business as usual”) greenhouse gas emissions scenario from the Intergovernmental Panel on Climate Change (IPCC) Fifth Assessment Report[25]. We chose the high-end scenario because it accentuates regional differences, which are more important for this analysis than absolute magnitudes. Figure 2 presents maps of the IPCC, GPCP, and irrigated area data.

Global Scale

By far the largest TWS trends occur in Antarctica (region 1; −127.6 ±39.9 Gt/yr averaged over the continent), Greenland (region 2; −279.0 ±23.2 Gt/yr), the gulf coast of Alaska (region 3; −62.6 ±8.2 Gt/yr), and the Canadian archipelago (region 4; −74.6 ±4.1 Gt/yr), where the warming climate continues to drive rapid ice sheet and glacier ablation[4, 5, 26, 27]. Positive trends in sub-regions of Antarctica and Greenland result from increasing snow accumulation[28]and millennial-scale dynamic thickening processes[29, 30]. Excluding those four ice-covered regions, one of the most striking aspects of changing TWS illuminated by Figure 1 is that freshwater seems to be accumulating in far northern North America (region 5) and Eurasia (region 6) and in the wet tropics, while the greatest non-frozen freshwater losses have occurred at mid-latitudes[8, 31]. The observed trends are consistent with increasing rates of precipitation during the period and the prediction of IPCC models that precipitation generally will decrease in mid-latitudes and increase in low and high latitudes by the end of this century[25]. They also complement recent studies that identify increasing rates of precipitation in the tropics and increasing water storage and river discharge in the high Arctic[12, 32]. However, because the rates of TWS change (0.45 ±0.43 cm/yr and 0.17 ±0.12 cm/yr in regions 5 and 6) and coefficients of determination (0.52 and 0.10) are small, while GIA related errors are relatively large, we cannot state definitively that these high latitude tendencies are real trends.

A second distinguishing characteristic of the map is that it reveals a clear ‘human fingerprint’ on the global water cycle. As seen in Figure 2, freshwater is rapidly disappearing in many of the world’s irrigated agricultural regions[6, 10, 33, 34, 35, 36, 37, 38]. A third aspect of the global trend map is natural interannual variability; many of the apparent trends are likely to be temporary, caused by oscillations between dry and wet periods (themselves driven by El Nino / La Nina and other climatic cycles) during the 14-year study period[39, 40].

Eurasia

The hotspot in northern India (region 7) was among the first non-polar TWS trends to be revealed by GRACE[41, 42]. It results from groundwater extraction to irrigate crops including wheat and rice in a semi-arid climate. Fifty-four percent of the area is equipped for irrigation. We estimate the rate of TWS depletion to be 19.2 ±1.1 Gt/yr, which is within the range of GRACE based estimates from previous studies of differently-defined northern India regions[41, 42, 43]. The trend persists despite precipitation being 101% of normal (compared with the 1979–2015 GPCP annual mean for the region) during the study period, with an increasing trend of 15.8 mm/yr. That extractions already exceed recharge during normal

NASA Author Manuscript NASA Author Manuscript NASA Author Manuscript

years does not bode well for groundwater during future droughts. The contribution of Himalayan glacier mass loss to the regional trend is minor[41, 42].

The increasing trend in central and southern India (region 8; 9.4 ±0.6 Gt/yr) likely reflects natural variability of (mostly monsoon) precipitation, which was 104% of normal with an increasing rate of 3.7 mm/yr (0.4%/yr). The m2 value is low (0.24), yet both trends are consistent with the IPCC-RCP8.5 predicted 23% precipitation increase by 2100.

The increasing trend in east-central China (region 9) is caused by a surge in dam construction and subsequent reservoir filling across that region[44]. Best known is the Three Gorges Dam Reservoir, which was filled to its design capacity of 39.3 Gt between June 2003 and October 2010[45]. The 14-year regional trend, 7.8 ±1.6 Gt/yr, did not change appreciably after the Three Gorges Dam Reservoir was filled. That can be explained by both the prevalence of other dam projects and greater precipitation after 2010 (971 mm/yr) than before (928 mm/yr). Further, seepage from dams tends to raise the regional water table, which can continue for years before the system equilibrates[46]. If precipitation trends towards an 8% increase by the end of this century, as predicted, then the observed TWS trend may persist even after the current dam building boom, though probably at a slower pace.

Satellite altimetry and Landsat data indicate that the majority of lakes in the Tibetan Plateau have grown in water level and extent during the 2000s, owing to a combination of elevated precipitation rates and increased glacier melt flows[47] that is difficult to disentangle. From 1997 to 2001 the average annual precipitation in region 10 was 160 mm/yr, well below the 2002–2015 average of 175 mm/yr, thus the observed increase in TWS (7.7 ±1.4 Gt/yr) may reflect replenishment after a prolonged dry period. Additional surface water storage would have been partially offset by glacier retreat and warming-enhanced evaporation. GIA may further complicate the partitioning of the GRACE derived mass change signal over the Tibetan Plateau[48], but some have argued that the GIA contribution is negligible[49]. The latter study noted that interannual mass variability in the region during the GRACE period is large relative to the inferred trend[49]. We concur ($r^2 = 0.67$) and conclude that there is no basis to extrapolate the apparent TWS trend into the future. In fact, it appears to have reversed in 2013 (Figure ED2). Although IPCC-RCP8.5 predicts a 20% increase in precipitation by 2100, it is probable that warming-induced glacier mass losses will begin to exceed surface water gains, particularly if the fraction of frozen precipitation decreases.

Region 11 lies to the west of the city of Urumqi in northwestern China’s Xinjiang province. During the study period TWS depletion was intense: −5.5 ±0.5 Gt/yr from an area of only 215,000 km^2. Precipitation data indicate drought was a nonfactor. The glaciers of the Tien Shan mountain range, whose central third lies within region 11, are melting rapidly[49], but not rapidly enough to explain all of the mass loss. Groundwater is being withdrawn to support irrigated agriculture across the province[50, 51] and possibly to dewater coal mines[52]. However, region 11 is contained within an endorheic basin. Hence the additional surface water produced by ice melt and groundwater abstraction cannot flow far, yet the elevations of the five lakes within that basin either declined or were stable during the study period, and GRACE did not detect significant TWS increases in other parts of the basin. We conclude that region 11 is losing glacier ice and possibly groundwater which ultimately become

NASA Author Manuscript NASA Author Manuscript NASA Author Manuscript

evapotranspiration, both in irrigated agricultural areas to the north, south, and west of the mountains and as evaporation from the desert floor to the south[50]. Details are provided in the supplementary Methods.

The vast agricultural region surrounding Beijing (region 12) is heavily irrigated (52%). Previous GRACE-based studies offered a wide range of estimates of groundwater depletion from the North China Plain aquifer (see the supplementary Methods for details), which is encompassed by region 12 and supports much of that irrigation. Here we estimate a TWS change rate of −11.3 ±1.3 Gt/yr for region 12. During the GRACE period annual total precipitation held steady, about 10 mm/yr above the 1979–2015 mean, following two dry years and a wet year during 2001–2003. All evidence suggests that this trend is human induced and likely to continue until groundwater becomes scarce or regulations are put in place to reduce consumption rates.

The negative trend that extends across East India, Bangladesh, Burma, and southern China (region 13), −23.3 ±1.9 Gt/yr, may be explained by a combination of intense irrigation[53] (25%) and a decrease in monsoon season precipitation during the period. Annual total precipitation was well above normal from 1998 to 2001, resulting in elevated TWS. During the GRACE period, precipitation declined at a rate of −10 mm/yr (−0.7%/yr), and the annual accumulations were below average from 2009 to 2015. This is the third most heavily irrigated of the study regions, so TWS decline is likely to continue, though perhaps at a slower rate given that rainfall should normalize eventually and a 15% increase in rainfall is predicted by 2100.

Decreasing water storage in the Middle East has been quantified using GRACE by previous studies[54, 55, 56]. Here we split the affected area into two regions, northwest Saudi Arabia (region 14; −10.5 ±1.5 Gt/yr) and the northern Middle East (region 15; including eastern Turkey, Syria, Iraq, and Iran; −32.1 ±1.5 Gt/yr). The declines result from a combination of recent drought and consequent increases in groundwater demand. Average precipitation during the study period was 78% and 96% of the 1979–2015 means in regions 14 and 15, with a slight declining trend (−1%/yr) in both. While the irrigation dataset indicates that less than 1% of region 14 is irrigated, Landsat imagery reveals the appearance and expansion of crop irrigation over the past three decades, supplied by non-renewable groundwater. However, the Saudi government ended their domestic wheat production program in market year 2014–15[57]. Thus while some farms have continued to operate, it is likely that the depletion rate in region 14 will diminish, and TWS may already be stabilizing (Figure ED2).

Region 15 has experienced a more complicated recent water history[54, 58]. Turkey's construction of 22 dams upstream on the Tigris and Euphrates Rivers in the last 3 decades has significantly decreased the rate of flow into Iraq and Syria. Combined with long-term drought, this has forced widespread over-reliance on groundwater for both domestic and agricultural needs and largely explains the large negative TWS trend[54, 59]. Surface and groundwater depletion is likely to continue in a stepwise fashion, with periods of near-stability during normal to wet years and rapid declines during drought years.

NASA Author Manuscript NASA Author Manuscript NASA Author Manuscript

To the north, an adjoining zone of TWS depletion (region 16; −18.1 ±1.3 Gt/yr) extends from the Ukraine through western Russia and into Kazakhstan. As before, the root cause is competition for scarce water resources, exacerbated by drought. Fifteen percent of the area is irrigated, including fertile croplands that are vital to Russia. Precipitation during the period was 97% of normal with a decreasing trend of 6 mm/yr (1%/yr). As in region 15, surface and groundwater depletion in region 16 is likely to continue as it has, stepwise, with substantial declines during drought years (2008, 2012, and 2014) and lesser recoveries in normal to wet years.

The water demands of regions 15 and 16 place severe pressure on the Aral and Caspian Seas[60] (regions 17 and 18). The demise of the Aral Sea is well known. Our estimate of the mass change in what remains of it is −2.2 ±0.1 Gt/yr. Water level fluctuations in the Caspian Sea have previously been attributed to meteorological variability[8] and direct evaporation from the Sea[61]. We find that annual discharge from the Volga River explains 60% of the variance in annual mean Caspian Sea level compared with 18% explained by evaporation from the Sea. Interannual variations in Volga River discharge are nearly three times as large as interannual variations in evaporation, and the former are controlled by both precipitation changes and the water demands of crops that cover 37% of the basin. Using crop production data and other information we establish that the −23.7 ±4.2 Gt/yr rate of change of water mass in the Caspian Sea observed by GRACE was caused in part by diversions and direct withdrawals of water from the rivers that sustain it (see the supplemental Methods for details), mirroring the circumstances that doomed the Aral Sea. The Caspian Sea contains about 78,000 Gt of water, so at the current rate it will survive for three more millennia, but a receding shoreline could be an issue.

Three mass changes that are prominent in Figure 1 in Eurasia are not associated with TWS at all. Crustal deformation accompanying the 2004, magnitude 9.1 Sumatra-Andaman earthquake caused two of the mass changes, the dipole positive and negative trends in Sumatra and the Malay Peninsula, respectively[62]. The 2011, magnitude 9.0 Tohoku earthquake caused the negative trend in Japan[63].

North America

Ongoing GIA processes centered near Hudson Bay, where the Laurentide ice sheet was thickest 20–95 thousand years ago, require a correction of the mass rates observed by GRACE of up to 5–6 cm/yr (equivalent height of water)[64, 65]. However, GIA models are imperfect and thus there is large uncertainty in the apparent decreasing TWS trend in central Canada (region 19) and some evidence that it may reflect an overcorrection of GIA[66]. Nevertheless, here we estimate the rate to be −7.0 ±6.4 Gt/yr. Loss of water would be consistent with a recent study that concluded Canada’s subarctic lakes are vulnerable to drying when snow cover declines, and that recent bouts of drying may be unprecedented in the past 200 years[67]. On the other hand, precipitation has been 102% of normal during the GRACE period, and a 17% increase is predicted by the end of the century.

The wetting trend in the northern Great Plains (region 20), 20.2 ±4.8 Gt/yr, arises from a combination of deep drought during 2001 to 2003, which greatly depressed water levels at

NASA Author Manuscript NASA Author Manuscript NASA Author Manuscript

the start of the GRACE period, followed by nine of the next eleven years having greater than average precipitation, including flooding in 2010–11[68]. The trend is likely to diminish over time although a 7% increase in precipitation is predicted by 2100.

A historically severe drought centered in southern California (region 21) that began in 2007 (ignoring a wet 2010) and consequent increases in groundwater demand[69, 70] conspired to diminish TWS at a rate of −4.2 ±0.4 Gt/yr. While atmospheric rivers during 2016–2017 replenished California's surface waters and policy changes have been enacted, it is doubtful that aquifer storage will recover completely absent significant usage reductions, in part because dewatering of aquifer materials can cause compaction of sediments, reducing aquifer capacity irrevocably[71]. In the Central Valley, which accounts for one third of the vegetables and two thirds of the fruits and nuts grown in the U.S., annual water demands for agriculture have exceeded renewable water resources since the early 20th century[71]. Groundwater well observations that extend back to 1962 suggest that each successive drought causes groundwater levels to step down to a new normal range without full recovery[71], as in regions 15 and 16. Declining winter snowpack in the Sierra Nevada Mountains, including a 500-year low in 2015[72], is a major concern because it is the main source of the region's surface water supply and groundwater recharge.

Sporadic droughts[73] in region 22, which encompasses parts of the southern High Plains and Texas, produced an apparent trend of −12.2 ±3.6 Gt/yr during the GRACE period. In this case we forecast partial replenishment. Large precipitation variations caused TWS to seesaw between high and low (Figure ED7). Heavy rains that led to flooding in parts of Texas and Oklahoma in May and October of 2015 and again in June of 2016 ended the most recent drought and reduced the linear rate of TWS decline during the GRACE period. On the other hand, withdrawals of groundwater that exceed recharge in the central and southern High Plains aquifer, to support irrigated agriculture, have persisted for decades[74] and will continue until the resource is exhausted or management policies change. The fringes of the aquifer have already run dry in places, and recent estimates predict that the southern High Plains aquifer could be depleted within 30 years[74]. Despite this situation, entrenched water rights are likely to preserve the status quo until the damage forces the hands of policymakers and stakeholders.

South America

Melting of the Patagonian ice fields (region 23) has previously been documented using altimetry[75] and GRACE[76]. Based on our analysis (see the supplemental Methods for details), TWS loss is occurring at a rate of −25.7 ±5.1 Gt/yr. In a warming world, melting of the Patagonian ice fields will continue until they are exhausted.

The magnitude 8.8 Maule (Chile) earthquake that occurred on 27 February 2010 is partly responsible for the apparent trend in Central Argentina[77] (region 24). A model has not yet been developed to properly separate its effect from TWS variations after that date (Figure ED3). TWS had previously been declining at a rate of −8.6 ±1.2 Gt/yr. The region received substantially elevated precipitation in five of the six years between 1999 and 2004, producing a TWS surplus at the start of the GRACE period. Multi-year drought began in

NASA Author Manuscript NASA Author Manuscript NASA Author Manuscript

2009, resulting in the observed April 2002 to February 2010 negative trend. TWS appears to have begun recovering (Figure ED3) in response to above-normal precipitation in 2014 and 2015 (Figure ED7), and we envisage that it will return to mean wetness conditions over time.

TWS increased during the GRACE period in central and western Brazil and its neighbors (region 25) at a rate of 51.9 ±9.4 Gt/yr. The region received less than average rainfall in every year from 2001 to 2005, followed by greater than average rainfall in six of the next ten years. As a result, TWS recovered from the early-period drought[78] and exhibited a massive but transitory increasing trend which may have already ended (Figure ED3). The magnitude is explained by both the size of the region and the intensity of the Amazon water cycle[79]. Still, we note that southern Brazil is a hotbed of dam construction[44], and it is possible that the filling of reservoirs contributed to the upward trend. Eastern Brazil (region 26) recently has suffered from a major drought[80], including well below normal rainfall in 2012, 2014, and 2015, causing TWS to plunge at a mean rate of −16.7 ±2.9 Gt/yr during the GRACE period. In both cases, assuming precipitation rates revert towards (or oscillate around) their long term means, the observed trends should fade. In fact, owing to the recent strong El Nino, 2015 was the driest year in the 37-year record for region 25 (Figure ED7), which may portend a reversion to average TWS.

Africa

Six apparent trends stand out in Africa. In southern Africa, a powerful wetting trend, 29.5 ±3.5 Gt/yr, encompasses the western Zambezi basin, the Okavango delta, and areas west to the coast (region 27). This region experienced a remarkable change in its hydroclimate. Area averaged annual rainfall was less than 970 mm in every year from 1979 to 2005. That threshold was exceeded five times from 2006 to 2011. A permanent climatic shift was previously speculated based on a significant decrease in annual precipitation between 1950–1975 and 1980–2005[81]. With ten years of additional hindsight, it appears that the region may simply have endured a prolonged drought from the late 1970s to the early 2000s. Thus, we attribute the GRACE period trend to natural variability[82]. Though TWS appears to have peaked in 2012 (Figure ED4), considering that the previous wet and dry periods lasted upwards of 25 years it is plausible that the wetting trend could resume.

An apparent trend of 21.9 ±3.9 Gt/yr occurs along the headwaters of the White Nile and Blue Nile Rivers, including Lakes Tanganyika and Victoria (region 28). Altimetry data indicate that during the study period both lakes experienced minimum water levels in 2006 and that their annual mean levels increased by 62 and 40 mm/yr on average, all of which is consistent with the TWS time series. Together, the two lake level trends equate to less than a quarter (4.8 Gt/yr) of the observed TWS trend. Considering that, rainfall would seem to be the primary driver of TWS variations, while management of the large lakes[83] and dam building in the northern part of the region[84] also contribute. However, rainfall is not particularly well correlated with either TWS or lake levels. The lack of correlation may be indicative of inaccuracies stemming from the sparsity of rain gauges in the region. The observed rainfall trend was negligible during the period, but a 12% increase is predicted by 2100. The northern part of region 28 encompasses the Grand Ethiopian Renaissance Dam on

NASA Author Manuscript NASA Author Manuscript NASA Author Manuscript

the Blue Nile River at Ethiopia's northwest border with Sudan, which Egypt has strongly denounced because of the possibility of reduced flow through the Nile. Construction of the dam began in 2011 and is ongoing. Filling of the 74 km^3 reservoir will likely produce a temporary increasing TWS trend in its immediate vicinity.

TWS has been increasing in tropical western Africa (region 29) at a rate of 24.1 ±2.1 Gt/yr. Precipitation was 3% below normal in 2000–2002 and 3% above during the rest of the GRACE period. This appears to be the primary cause of TWS accumulation, though the possible contribution of the many dams being built in this part of Africa[44] is unknown. Interannual variability of rainfall is substantial in the region[85], so disregarding the dams, it is likely that the rate of change of TWS will oscillate around zero over the coming decades. By 2100 rainfall is predicted to decrease by 6%, hence the dam construction may be timely.

Decreasing TWS (−7.2 ±1.0 Gt/yr) in region 30, which extends from the coast of central Africa into the northern Congo River basin, seems to be caused by natural interannual variability, though it has been suggested that the surface runoff rate has been enhanced by deforestation[84]. Between 1999 and 2002 rainfall averaged 4% above normal, while it averaged 1% below normal during the rest of the GRACE period, including two very dry years in 2014 and 2015. The decrease in TWS also happens to be consistent with the postulated negative correlation between TWS in the Amazon and Congo basins[86], which further implicates large scale climatic oscillation as the ultimate driver[85].

The negative trend along the coast of southeastern Africa (region 31), −12.9 ±2.3 Gt/yr, reflects a recent severe drought[79] which has caused major food shortages. Rainfall was 4% below average during the GRACE period, including annual accumulations that were below normal in five of the last eight years and barely above normal in the other three. Water levels in Lake Malawi, which is in the center of the region, are well correlated with regional TWS. The lake declined at a mean rate of 78 mm/yr during the period, accounting for 2.3 Gt/yr of the observed TWS trend. Thus it is likely that the apparent trend is primarily caused by natural variability[84], though a 6% decrease in rainfall is predicted during this century.

A weak negative trend, −11.7 ±2.9 Gt/yr, extends across arid Africa north of 19°N excluding Morocco (region 32). The coefficient of determination is not large at 0.45, nevertheless, precipitation during the GRACE period was 7% above normal, which suggests that the consumptive use of fossil groundwater to stimulate agriculture and economic development is the cause[55, 84, 87] Three studies[6, 10, 36] estimated recent rates of consumptive groundwater use across North Africa to be 7.8, 15.7, and 4.1 Gt/yr, bracketing our TWS depletion estimate.

Australia

Australia appears to be bipolar with respect to water storage during the GRACE era, with wetting in the east and north and drying in the northwest. The worst drought in over 100 years afflicted eastern Australia during 2001–09[88]. It is likely that groundwater was more heavily consumed during that time to compensate for reduced availability of surface waters. Recovery from the drought began with heavy rains in 2010 and transitioned to severe

NASA Author Manuscript NASA Author Manuscript NASA Author Manuscript

flooding in 2011, with so much water stored on the continent in 2012 that global mean sea level temporarily declined[89]. The shift from dry to wet conditions caused the apparent wetting trend in region 33, 19.0 ±2.8 Gt/yr, but most of that water had already been shed by 2016 (Figure ED4). North Western Australia received greater than normal rainfall during every year from 1997 to 2001, including the two wettest years in the GPCP record in 2000 and 2001. Thus region 34 began 2002 near maximum TWS capacity, and it gradually returned to average[90] (−8.9 ±1.2 Gt/yr) with 99% of normal precipitation during the GRACE period. It is possible that aquifer dewatering associated with Pilbara's mining industry also contributed, but reliable data are not available to confirm and quantify that contribution. We can only justifiably conclude that natural variability is the primary explanation for both Australian trends.

Implications and Discussion

GRACE has revealed significant changes in freshwater resources occurring across the globe, and has enabled them to be quantified at regional scales, unimpeded by sparse measurements or restrictive data access policies. Some of these changes are manifestations of human water management that, prior to GRACE, were known only anecdotally, including TWS depletion in northern India, the north China plain, and the Middle East (regions 7, 12, 14–16), or not at all, as in northwestern China (region 11). They portend a future in which already limited water resources will become even more precious. Others correlate well with global warming and predicted future precipitation changes, including worldwide ice sheet and glacier melt (regions 1–4, 23) and TWS increases in the northern high latitudes (regions 5–6). Apparent TWS trends in about one-third of the study regions represent partial cycles of longer term interannual oscillations, and may well fade or reverse over the decades (see green dots in Figure 1). While we have made every effort to attribute the apparent trends properly, all will require continued observation to better understand their causes and constrain their rates.

The GRACE data provide motivation for multilateral cooperation among nations, states, and stakeholders, including development of transboundary water sharing agreements, to balance competing demands and defuse potential conflict[33]. Government policies that incentivize water conservation could help to avert a "tragedy of the commons" scenario, i.e., opportunistic competition for groundwater outweighing the altruistic impulse to preserve the resource. Northern India, the North China Plain, the Middle East, and the area surrounding the Caspian Sea are already on a perilous path, while California, in response to severe drought and alarming groundwater declines in the Central Valley, recently passed legislation to regulate groundwater consumption.

In many regions, crop irrigation on massive scales has been supported by unsustainable rates of groundwater abstraction[6, 33, 33, 34, 91]. In the face of aquifer depletion, population growth, and climate change, water and food security will depend upon water saving technologies and improved management and governance. The success of such an approach in arid Israel[92] proves that a comprehensive water conservation strategy can work, and there are encouraging signs in Saudi Arabia (as previously discussed) and parts of India[93] as well. Meanwhile, as China looks to improve living standards for its 1.38 billion residents, it will

NASA Author Manuscript NASA Author Manuscript NASA Author Manuscript

continue to face daunting water management decisions, many related to massive geoengineering and water diversion projects that are likely to trigger political tensions.

The GRACE data also call attention to regions where continued monitoring will be essential for distinguishing, understanding, and quantifying climate change impacts on the water cycle[94, 95] and groundwater[96, 97] in particular. This is important for two reasons. First, verification of emerging hydroclimatic trends such as increasing northern high latitude precipitation would raise confidence in the ability of climate models to predict water cycle consequences of climate change[98]. Second, a redistribution of freshwater from dry to wet regions, as has been forecast, could exacerbate disparities between the water “haves” and “have nots” and associated political instability, migration, and conflict. Most groundwater depletion is occurring within Earth’s mid-latitudes, resulting in a positive drying feedback that is accelerating water losses and the severity of related socioeconomic issues[33].

New and future satellite remote sensing missions that extend the long term record of global, hydrological observations will be essential for continued assessment of changing freshwater availability[99]. In particular, the GRACE Follow On mission (planned to launch in early 2018), while affording a small increase in spatial resolution/accuracy[100], will enable surveillance of the trends described here and improved disentanglement of natural TWS variability from hydroclimatic change. Awareness of changing freshwater availability (e.g., Figure 1) is the first step towards addressing the challenges discussed here, through improved infrastructure, water use efficiency, lifestyle and water management decisions, and policy.

Methods

GRACE data have traditionally been processed by solving for gravity anomalies in terms of Stokes coefficients[101, 102, 103, 104, 105, 106]. These solutions suffer from correlated errors that manifest as longitudinal striping in the gravity solution, requiring tailored “destriping” and smoothing post-processing filters to remove[107]. While largely successful in removing errors, the post-processing also damps and smooths real geophysical signals[101]. Recent advances in GRACE data processing have shown that solving for gravity anomalies in terms of mass concentration (`mascon’) functions with carefully selected regularization results in superior localization of signals on an elliptical Earth[4, 21, 108, 109]. For instance, mascon solutions correlate better with in-situ ocean bottom pressure recorders than spherical harmonic solutions[21, 109], improve the spatial resolution of mass changes in Greenland[29], and were used to detect changes in the Atlantic Meridional Overturning Circulation[110]. Currently, there are three publicly available GRACE mascon solutions: Jet Propulsion Laboratory mascons RL05M.1 version 2[21, 111] (JPL-M), Center for Space Research mascons RL05M[109] (CSR-M), and Goddard Space Flight Center mascons version 2.3b[4] (GSFC-M). JPL-M parameterizes the gravity field with 4,551 equal-area 3° mascon elements, while CSR-M and GSFC-M both parameterize the gravity field in terms of 1° mascon elements (−41,000 mascon elements are solved for in each solution). The implementation details of each mascon solution differs, but we note that the JPL solution has the unique characteristic that each 3° mascon element is relatively uncorrelated with neighboring mascon elements, while the 1° mascon elements in the CSR and GSFC are highly correlated with their neighbors.

NASA Author Manuscript NASA Author Manuscript NASA Author Manuscript

Three degrees corresponds approximately to the ‘native’ resolution of GRACE, and being uncorrelated with one another in the retrieval allows for a quantitative understanding of leakage errors when aggregating mass anomalies within a hydrological basin[112]; in fact, no literature yet exists on quantifying leakage errors in 1° mascon solutions. As such, in this manuscript, we use the JPL RL05M GRACE mascon solution for trend analysis and mapping; however, we use all (i.e., JPL-M, CSR-M, and GSFC-M) mascon solutions to derive uncertainties.

The JPL RL05M GRACE mascon solution parameterizes each monthly gravity field in terms of 4,551 equal-area surface spherical cap mass concentration functions, and uses a regularization approach that implements both spatial and temporal correlations to remove correlated errors during the gravity inversion. A Coastline Resolution Improvement (CRI) filter is used to separate between land and ocean mass within mascons that span coastlines[112]. GRACE does not produce a reliable estimate of the Earth’s oblateness (C20 coefficient), and as such, we follow the standard protocol of using Satellite Laser Ranging to provide this estimate[113]. Further, GRACE gravity field anomalies are measured in the center of mass Earth reference frame, and therefore need to be augmented with a ‘geocenter’ estimate to capture all surface mass changes[114]. GIA corrections are made using the updated ICE-6G D model[64, 65], with an exception for Antarctica, for which we reduce the fitted rate of mass change by 9.2 Gt/yr based on a regional model[115] that potentially provides a better GIA estimate for Antarctica[116]. Finally, corrections are made to the C21 and S21 coefficients[117] in order to fully remove the pole tide from the GRACE data. Jumps in the background atmosphere and ocean dealiasing product are corrected as well[118].

Prior to computing the best fit linear trend from a TWS time series, the seasonal cycle was removed as follows. First, missing months of data were filled by linear interpolation. Next, the mean monthly seasonal cycle was computed by averaging all Januarys, all Februarys, etc. Finally, for each month in the original, non-gap-filled time series, the mean for the corresponding month of the year was subtracted. The first step, gap filling, was necessary because, for example, the month of May was under-sampled in the second half of the study period, which caused the mean May to be biased in locations where a consistent trend existed (i.e., most of the regions of this study).

Trend error estimates account for both systematic and random GRACE measurement errors as well as systematic GIA model error. GRACE measurement error is taken to be the 1-sigma standard deviation between trend estimates obtained from JPL-M, CSR-M, and GSFC-M. Given the specific basin boundaries used in this study, we find JPL-M to have more pronounced trends (both positive and negative) than CSR-M and GSFC-M, which is consistent with previous conclusions[119]. This spread is due to a fundamental difference in the spectral content between the 3° mascons and 1° mascons, implying that leakage characteristics are different when aggregating mass anomalies over a particular region (somewhat counter-intuitively, the 3° mascons ‘focus’ more signal than the 1° sampled mascons). In essence, the ‘smooth’ nature of the 1° mascon solutions (CSR-M and GSFC-M) results in significant damping of signal over our regions of interest due to leakage across the basin boundaries. For a more direct comparison of the three solutions over our regions of interest, we matched the spectral content of JPL-M to that of CSR-M. The regularization of

NASA Author Manuscript NASA Author Manuscript NASA Author Manuscript

the CSR mascon solution is based on a 200 km Gaussian smoothed representation of a regularized spherical harmonic solution[109]; hence, it is expected that the final mascon solution will inherit some of these spectral characteristics. Thus, we smooth JPL-M with a Gaussian filter with a 200 km radius, and compare trend estimates of the smoothed version of JPL-M to CSR-M and GSFC-M. The agreement is now significantly better, and trends in the smoothed version of JPL-M are now also damped similarly to CSR-M and GSFC-M (see Figure ED9 for an example). Analog analysis has been performed before by others in studying mass variations over the Caspian Sea[120]. We use the 1-sigma standard deviation of trend estimates obtained from the smoothed version of JPL-M, CSR-M, and GSFC-M to derive the GRACE measurement errors. GIA model error is taken to be the 1-sigma spread between four competing GIA models[64, 65, 121, 122, 123, 124] that implement two distinct loading histories, four distinct viscosity profiles, and different implementation of physics. The uncertainty on the trend for any region is given by the root sum of squares combining the GIA model error (which only manifests as a trend) and the GRACE measurement error.

Time series for the Aral and Caspian Seas (regions 17 and 18) were calculated by applying a set of gain factors to the GRACE data. Gain factors act to redistribute mass within each individual mascon (at sub-mascon resolution), allowing for exact averaging kernels to be applied to a region of interest and retrieval of accurate, unbiased (by leakage) mass change values[112,125]. These particular gain factors were derived[112] via a combination of total column soil moisture output from the Noah land surface model driven by the Global Land Data Assimilation System[100] (which does not include sea water variations) along with altimetry data[127] over the Seas.

Recent variations in Caspian Sea Level have been attributed by previous studies to natural meteorological variability[8] and direct evaporation from the sea surface[61]. We tested these two theories and a third, agricultural water consumption. Flow in the Volga River, which delivers roughly 80% of the runoff to the Caspian Sea, is controlled by a series of eleven dams[128]. Among other purposes these ensure a steady supply of water for crop irrigation[128]. Data to quantify interannual variations in irrigation extent, intensity, or volumes in the Caspian Sea drainage basin during the study period were not available. Estimates of Russian wheat, maize, rice, and soybean annual production[129] (in tons) during 1992–2015 were obtained from the Organisation for Economic Co-operation and Development (OECD). According to the irrigation dataset[23], the Volga River basin, which drains to the Caspian Sea, includes 3% irrigated crops and 37% rain-fed crops by area, and it accounts for about half of all Russian crop production, so the latter is a fair but imperfect indicator of agricultural water demand in the basin. Yearly total production was normalized by subtracting the 24-year mean and dividing by the standard deviation. Normalization was similarly performed on annual time series of GPCP precipitation[22] over the Caspian Sea and Volga River drainage basins, Volga River discharge, reanalysis based Caspian Sea evaporation[130], and changes in Caspian Sea level from satellite altimetry[24]. Correlation coefficients (and significance levels) between normalized Caspian Sea level change and its significant drivers (Figure ED10) were 0.78 (Volga River discharge; $p<0.001$), −0.47 (crop production; $p=0.02$), −0.43 (Caspian Sea evaporation; $p=0.04$), and 0.41 (Caspian Sea drainage basin precipitation; $p=0.05$). Correlation coefficients (and significance levels) between normalized Volga River discharge and significant drivers were 0.52 (Volga River basin precipitation;

NASA Author Manuscript NASA Author Manuscript NASA Author Manuscript

p=0.01) and −0.40 (crop production; p=0.06). Notably, the correlation between crop production and precipitation was negligible, suggesting that irrigation effectively mitigates the impact of drought. Interannual variations in Caspian Sea evaporation do, indeed, contribute significantly to Caspian Sea level changes. However, annual Volga River discharge variations are better correlated with annual changes in Caspian Sea level, they are larger than variations in Caspian Sea evaporation (standard deviation of 48 Gt vs. 18 Gt, compared with 38 Gt mean magnitude of annual Caspian Sea level change), and they are controlled by both precipitation and rising agricultural water demand[128]. We therefore conclude that all three factors contributed to the observed water loss (−23.7 ±4.2 Gt/yr based on GRACE, ignoring steric effects; −25.4 Gt/yr based on satellite altimetry) during 2002–2015.

For the Gulf Coast of Alaska and Patagonian Ice Fields (regions 3 and 23) it was also necessary to increase the rates of mass loss (by 7 Gt/yr and 9 Gt/yr, respectively) to account for Little Ice Age GIA[31]. Note the full GIA corrections to Antarctica, the Gulf Coast of Alaska, and the Patagonian Ice Fields are not incorporated into Figures ED1 and ED3.

The irrigated area percentages (Table 1) were computed by area-weighted averaging of the individual pixel values of irrigation intensity[23] (%) within each study region. Precipitation trends (mm/yr) were computed based on monthly data[22] as above for TWS, except that there were no gaps to fill. Precipitation trends (%/yr) and precipitation percentages of normal were computed using the 1979–2015 annual mean precipitation totals for each region. Predicted precipitation changes were computed as area weighted averages from the IPCC dataset[25] over the study regions. The precipitation maps in Figure 2 were computed as above but on a pixel by pixel basis.

The explanation for the mass loss trend in northwest China (region 11), −5.5 ±0.5 Gt/yr, is complex. Drought was not a factor given that precipitation was 10% above normal and stable during the period. Two recent studies[131, 132] estimated the rate of glacier loss over the entire Tien Shan mountain range to be −5.4 ±2.9 Gt/yr and −7.5 ±3.4 Gt/yr based on Ice, Cloud and Land Elevation Satellite (ICESat) observations from 2003 to 2009. These estimates are somewhat smaller than our GRACE based estimate of TWS decline in region 11 during that period (−8.3 ±0.8 Gt/yr), despite region 11 encompassing less than half of the area of glacier melt[131]. Thus we conjecture that an additional catalyst for mass loss must exist. Xinjiang province is one of the world’s largest producers of coal, having an estimated 2.2 trillion tons of reserves[133]. Reported rates of coal removal and burning themselves are more than an order of magnitude smaller than the GRACE-observed mass loss[133], but mining involves dewatering of the aquifers that the mines intersect. Consequent groundwater depletion in the area is possible[52] but unconfirmed. Adding to the complexity, region 11 lies within a larger, endorheic basin, meaning that water pumped from the ground or melting from glaciers will remain as surface water, become groundwater recharge, and/or evapotranspire, as opposed to flowing to the ocean. However, based on satellite altimetry data, the elevations of the five lakes within the surrounding endorheic basin did not increase during the study period. All either declined or did not change significantly. The two lowlands into which region 11 drains (one northwest, one southeast) have GRACE-based trends of 0.3 and −0.6 Gt/yr (both insignificant). Ultimately evapotranspiration must account for the water lost from region 11.

NASA Author Manuscript NASA Author Manuscript NASA Author Manuscript

The average annual precipitation in region 11 is 194 mm/yr, making it the fourth driest of the 32 study regions. The endorheic basin is extensively irrigated, including 7% of region 11, and irrigation intensity is likely rising in support of Xinjiang province's population growth (18.2 million to 21.8 million between 2000 and 2010)[51]. Massive amounts of surface water from Lake Bosten and the Kongque River (both southeast of region 11) are transferred via aqueducts southward to the Tarim River in order to support farming in the arid plains, yet the Tarim River runs dry before reaching its natural terminus, Lop Nor lake[50]. To summarize, the Tien Shan mountain glaciers in region 11 are shrinking due to global warming. Groundwater may be declining due to agricultural withdrawals and/or mining operations, but the latter is unconfirmed. Because region 11 lies within an endorheic basin, neither glacier melt nor groundwater pumping can alone explain the observed TWS depletion. The corollary is that the resulting additions to surface water are balanced by desert-and irrigation-enhanced evapotranspiration.

As noted in the main text, previous GRACE based studies of the North China Plain (region 12), while agreeing that groundwater depletion associated with intense irrigation was the cause, offered a wide range of estimates of the TWS or groundwater trend. Specifically, put into common units, these estimates equated to −8.3 Gt/yr over a 370,000 km^2 area[134], −35 Gt/yr over a 2,086,000 km^2 area[135], −2.33 Gt/yr over a 370,000 km^2 area[136], and −14.09 Gt/yr over a 1,500,000 km^2 area[137], compared with our estimate of −11.3 Gt/yr over a 876,004 km^2 area.

Data Availability

Specific sources of data used in this study were the following. The primary GRACE TWS dataset is JPL Mascon RL05M.1 version 2 was accessed 3 February 2017 from https://grace.jpl.nasa.gov/data/get-data/jpl_global_mascons/. Additional GRACE TWS datasets used to estimate errors were CSR RL05 Mascon version 1 accessed 20 September 2017 from http://www2.csr.utexas.edu/grace/RL05_mascons.html and GSFC Mascon version 2.3b accessed 5 October 2017 from https://neptune.gsfc.nasa.gov/gngphys/index.php?section=413. Primary GIA data used in this study were the ICE-6GD model accessed 1 December 2017 from http://www.atmosp.physics.utoronto.ca/~peltier/data.php and the IJ05_R2 GIA correction for Antarctica accessed 3 February 2018 from http://onlinelibrary.wiley.com/doi/10.1002/jgrb.50208/full. Additional GIA data used to compute GIA model error included ICE-6G_ANU_D accessed 3 February 2018 from http://onlinelibrary.wiley.com/doi/10.1002/2017JB014930/full, the A et al. (2013) GIA model accessed 16 December 2013 from ftp://podaac-, and the Paulson et al. (2007) GIA model accessed 3 February 2018 from https://academic.oup.com/gji/article/171/2/497/2018541. Atmosphere and ocean dealiasing product jump corrections were accessed 13 June 2016 from ftp://podaac-ftp.jpl.nasa.gov/allData/grace/docs/. GPCP version 2.3 precipitation data were accessed 23 September 2016 from https://www.esrl.noaa.gov/psd/data/gridded/data.gpcp.html. Global Rain-fed Irrigation and Paddy Croplands version 1 data were accessed 12 September 2016 from http://ftp- earth.bu.edu/public/friedl/GRIPCmap/. Global Reservoirs/Lakes elevation version TPJO.2.3 data were accessed 29 July 2016 from https://ipad.fas.usda.gov/cropexplorer/global_reservoir/. IPCC 5th Assessment Report (RCP8.5) predicted precipitation change data were accessed 1 September 2016 from https://

NASA Author Manuscript

NASA Author Manuscript

NASA Author Manuscript

www.ipcc.ch/pdf/assessment-report/ar5/wg1/WG1AR5_AnnexI_FINAL.pdf. Russian crop production data were accessed 16 August 2017 from https://data.oecd.org/agroutput/crop-production.htm. Latent heat flux (evapotranspiration) data for the Caspian Sea and its drainage basin were extracted from MERRA2 Land Surface Diagnostics version M2TMNXLND_5.12.4, accessed 19 September 2017 from https://disc.sci.gsfc.nasa.gOv/datasets/M2TMNXLND_5.12.4/summary. Volga River discharge observations are restricted from public access, but a time series of normalized annual discharge values was provided to M.R. by Valentina Khan of the Hydrometeorological Research Center of the Russian Federation.

The JPL RL05M GRACE solution used in this study is identical to that which is available from the NASA/JPL GRACE Tellus website with exception that we implemented a different GIA model, a correction to the pole tide, and corrections to the background atmosphere/ocean dealiasing model. These adjustments are available from D.N.W. upon request. Data analyzed to create Figure ED9 are available from D.N.R. upon request. Excel spreadsheets containing the data and calculations used to create Table 1 and Figure ED10 are available from M.R. upon request.

Code Availability

GRACE based TWS time series for the study regions were prepared, including GIA adjustments, C21 and S21 coefficient replacements, and corrections due to jumps in the atmosphere and ocean dealiasing products, using MATLAB scripts. These are available upon reasonable request from D.N.W. TWS time series analyses, including trend estimation and r^2 computation, were performed within Excel spreadsheets, which are available from M.R. upon reasonable request.

NASA Author Manuscript

NASA Author Manuscript

NASA Author Manuscript

Extended Data

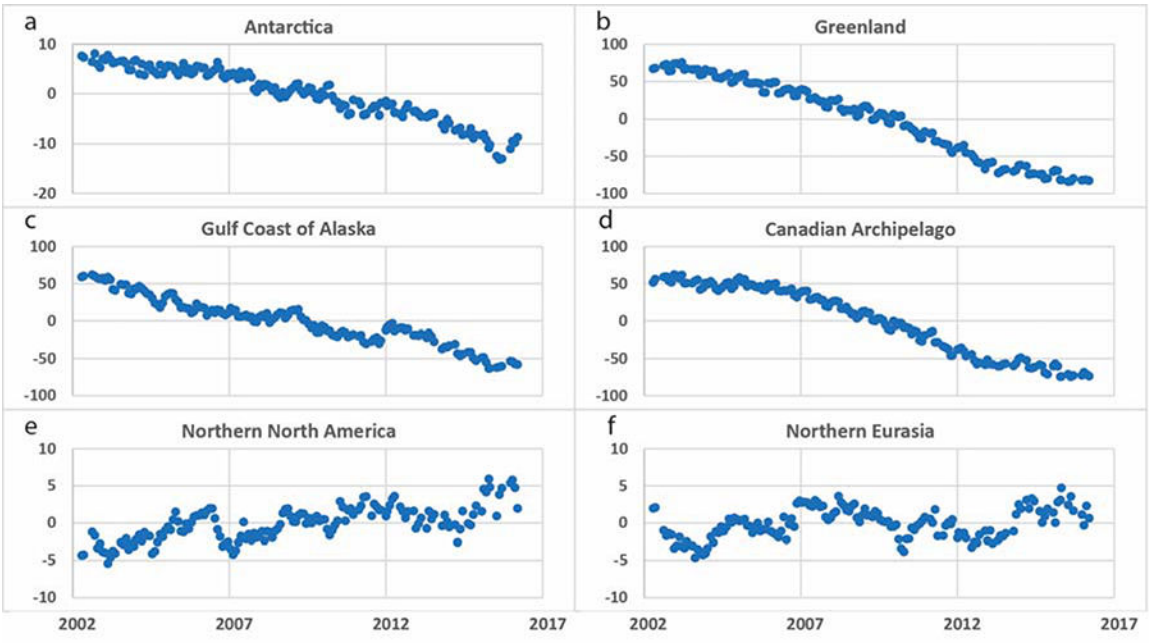

Figure ED1. Non-seasonal TWS anomalies: global regions.

Time series of monthly TWS anomalies (departures from the period mean) from GRACE, after removing the mean seasonal cycle, averaged over each of study regions 1–6 (panels a-f), as equivalent heights of liquid water (cm). Note that the y-axes vary among panels.

NASA Author Manuscript

NASA Author Manuscript

NASA Author Manuscript

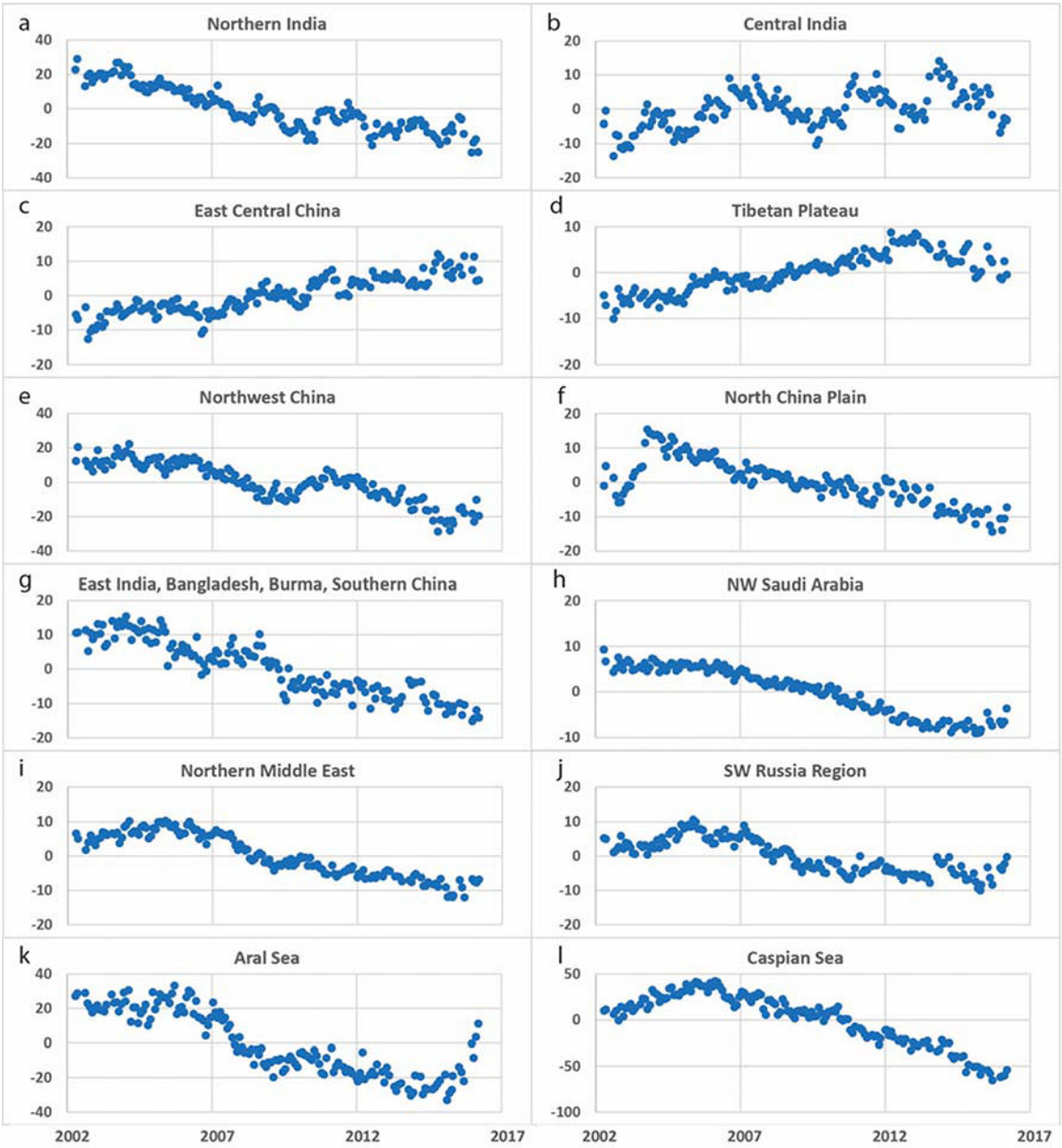

Figure ED2. Non-seasonal TWS anomalies: Eurasia

As in Figure ED1, for regions 7–18 (panels a-l).

NASA Author Manuscript

NASA Author Manuscript

NASA Author Manuscript

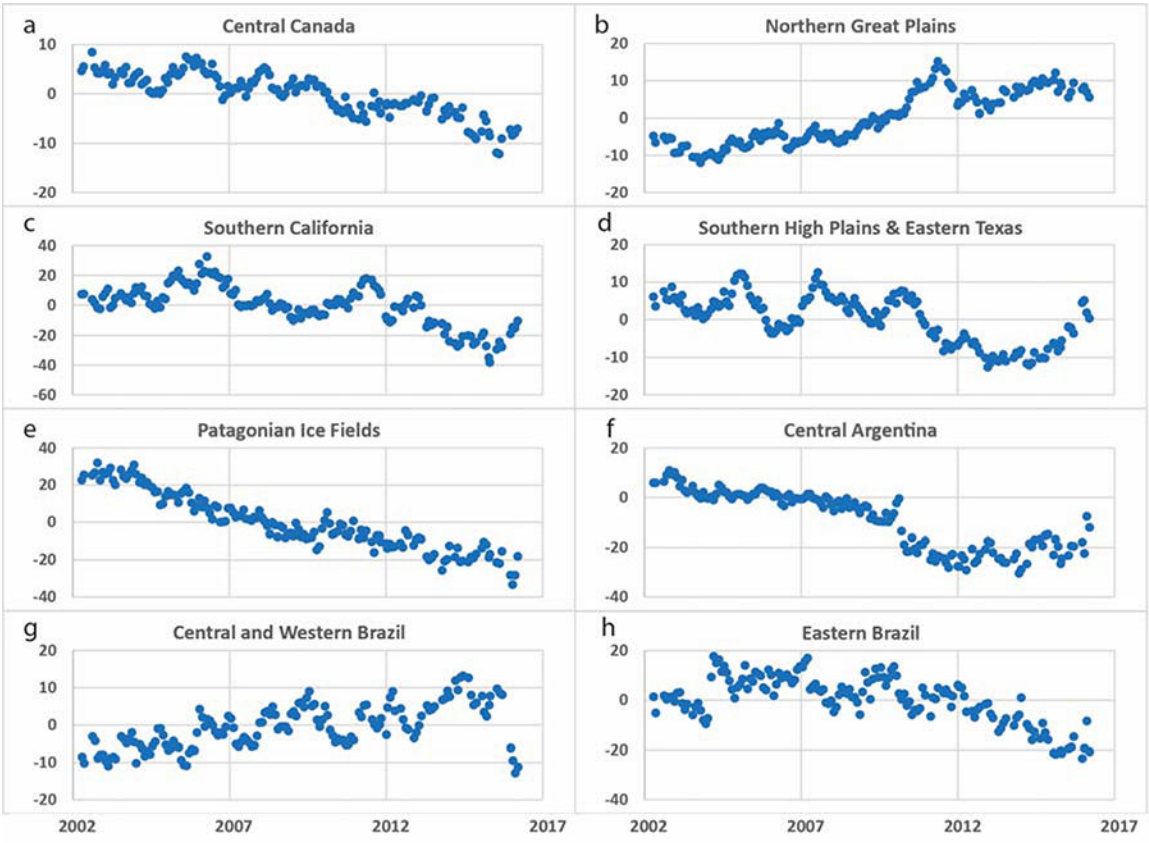

Figure ED3. Non-seasonal TWS anomalies: North and South America.
As in Figure ED1, for regions 19–26 (panels a-h).

NASA Author Manuscript

NASA Author Manuscript

NASA Author Manuscript

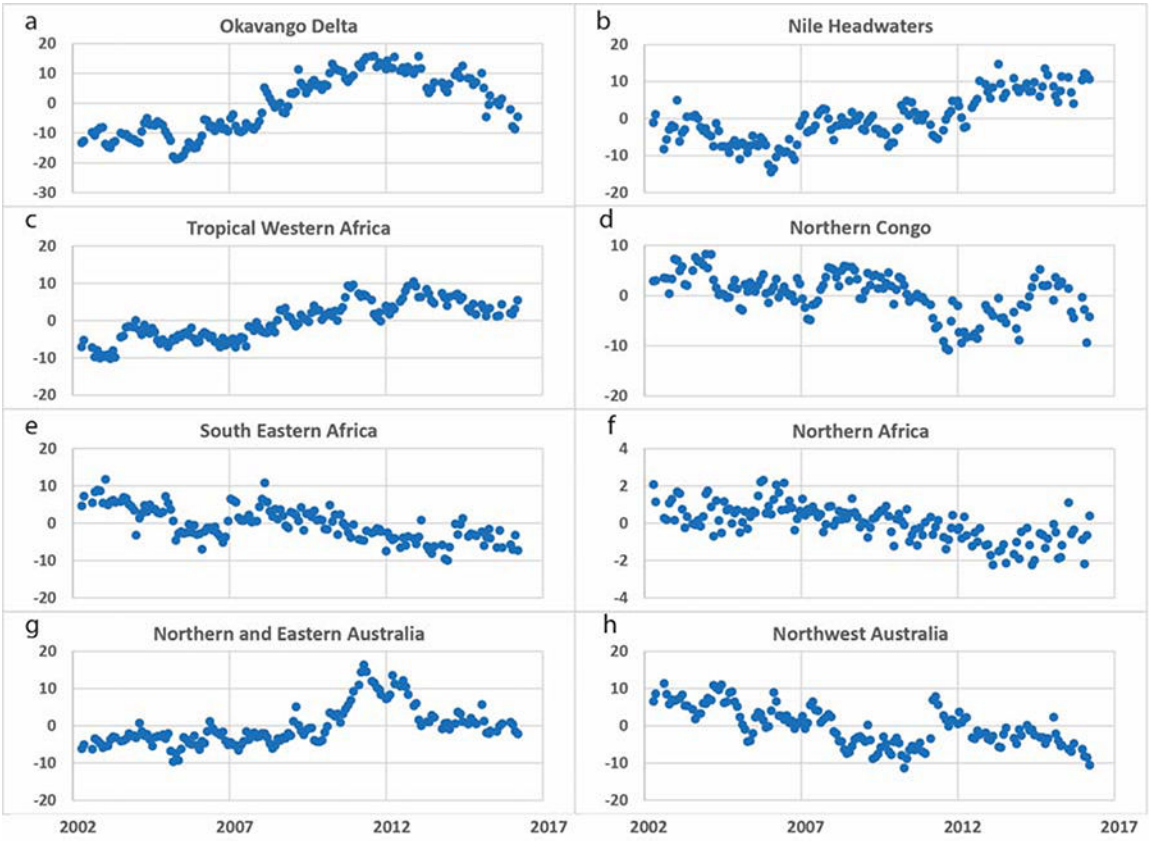

Figure ED4. Non-seasonal TWS anomalies: Africa and Australia.
As in Figure ED1, for regions 27–34 (panels a-h).

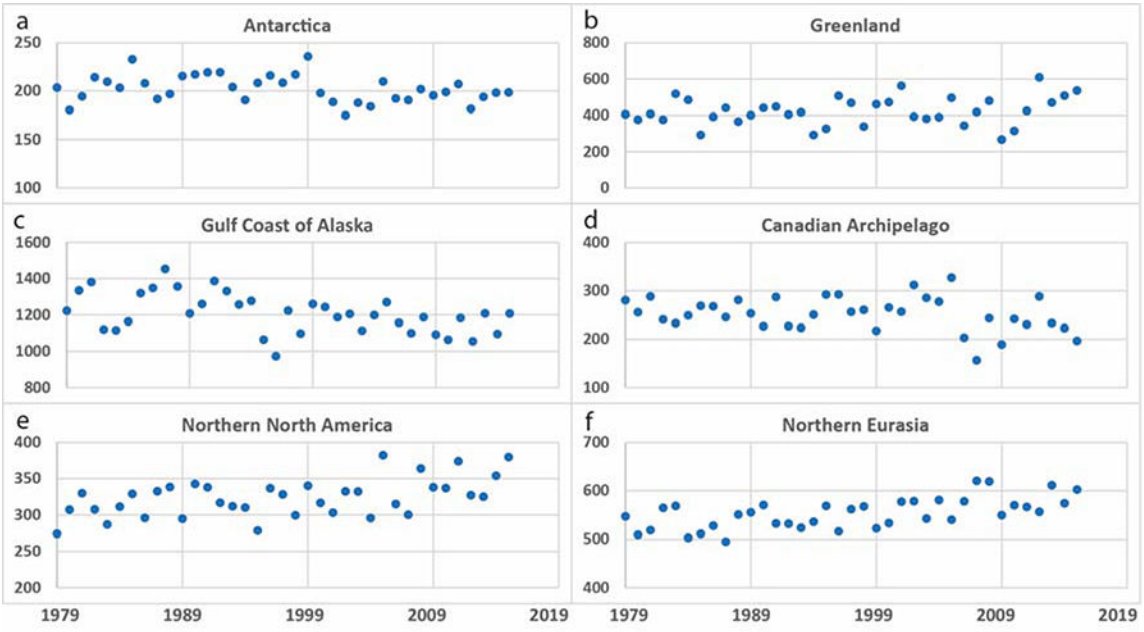

Figure ED5. Annual precipitation totals: global regions.

NASA Author Manuscript

NASA Author Manuscript

NASA Author Manuscript

Time series of annual precipitation totals (mm) averaged over each of study regions 1–6 (panels a-f), based on GPCP v.2.3. Note that the y-axes vary among panels.

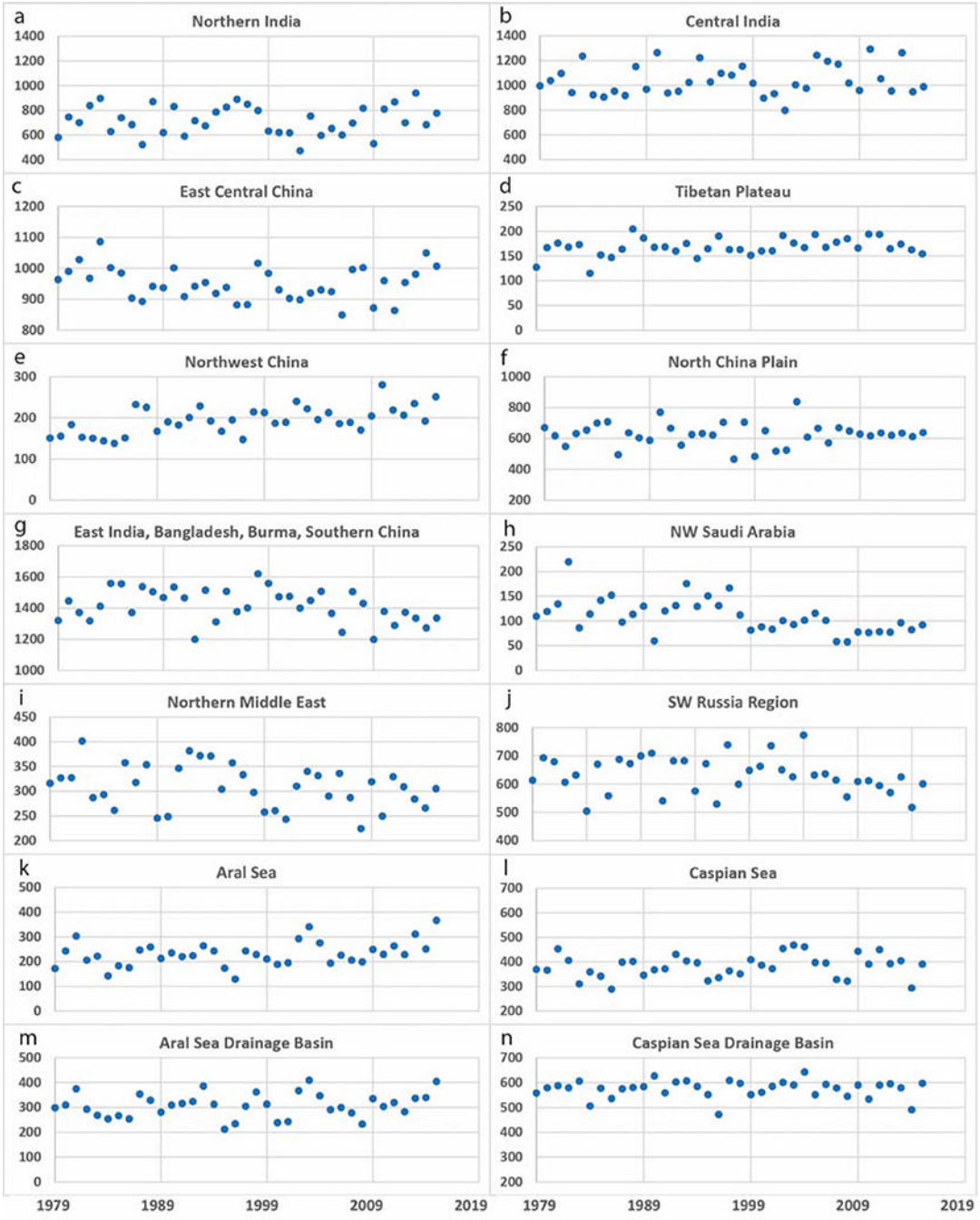

Figure ED6. Annual precipitation totals: Eurasia.

As in Figure ED5, for regions 7– 18 and the full drainage basins of the Aral and Caspian Seas (panels a-n).

NASA Author Manuscript

NASA Author Manuscript

NASA Author Manuscript

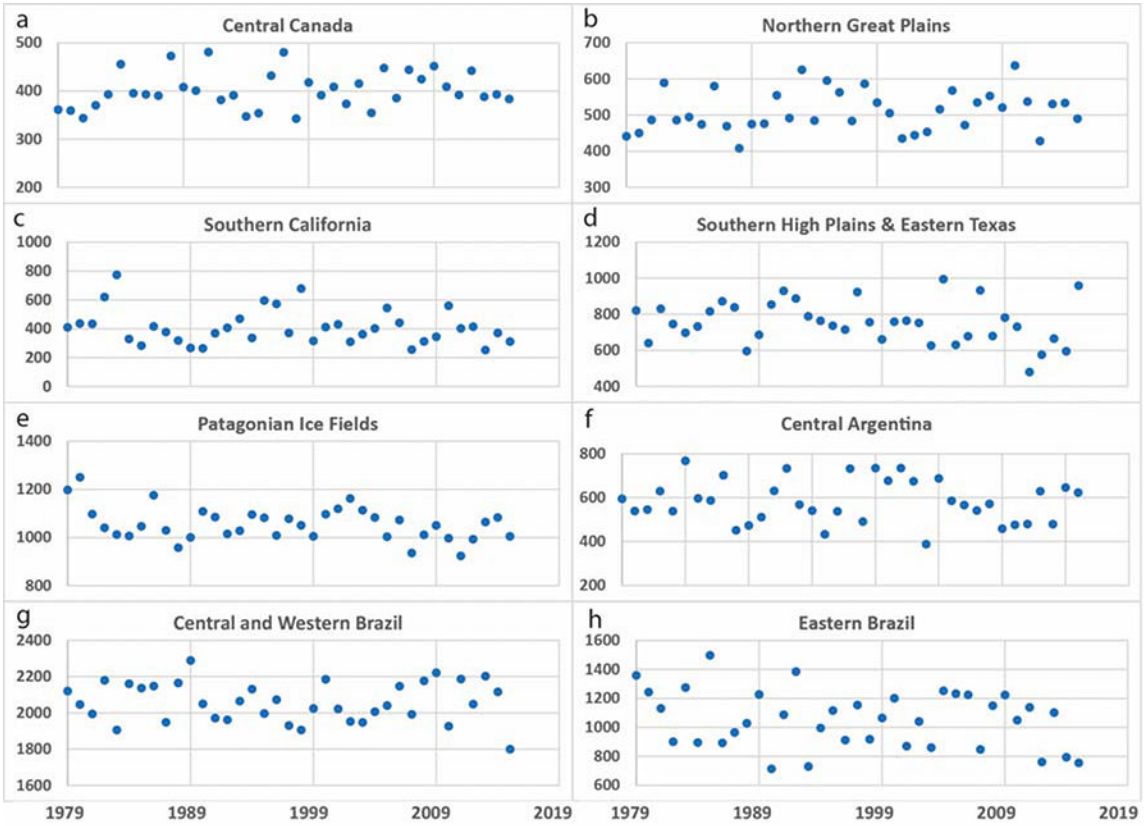

Figure ED7. Annual precipitation totals: North and South America.
As in Figure ED5, for regions 19–26 (panels a-h).

NASA Author Manuscript

NASA Author Manuscript

NASA Author Manuscript

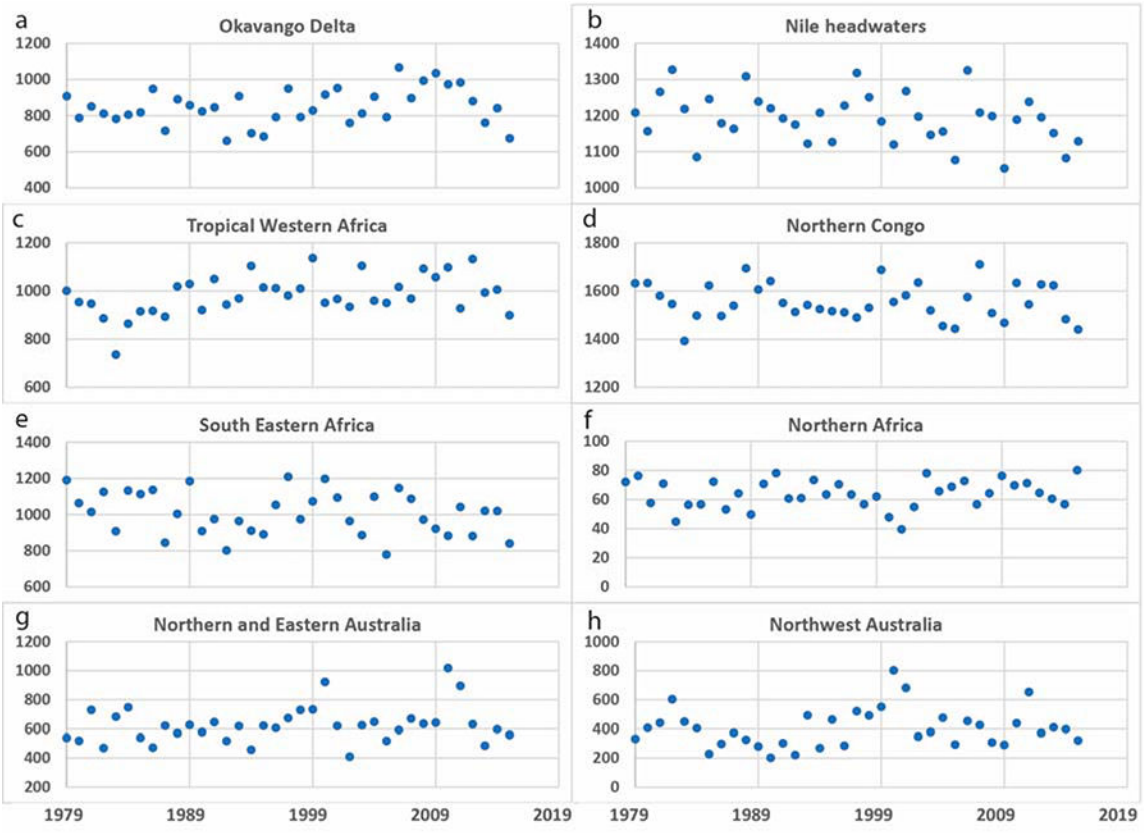

Figure ED8. Annual precipitation totals: Africa and Australia.
As in Figure ED5, for regions 27–34 (panels a-h).

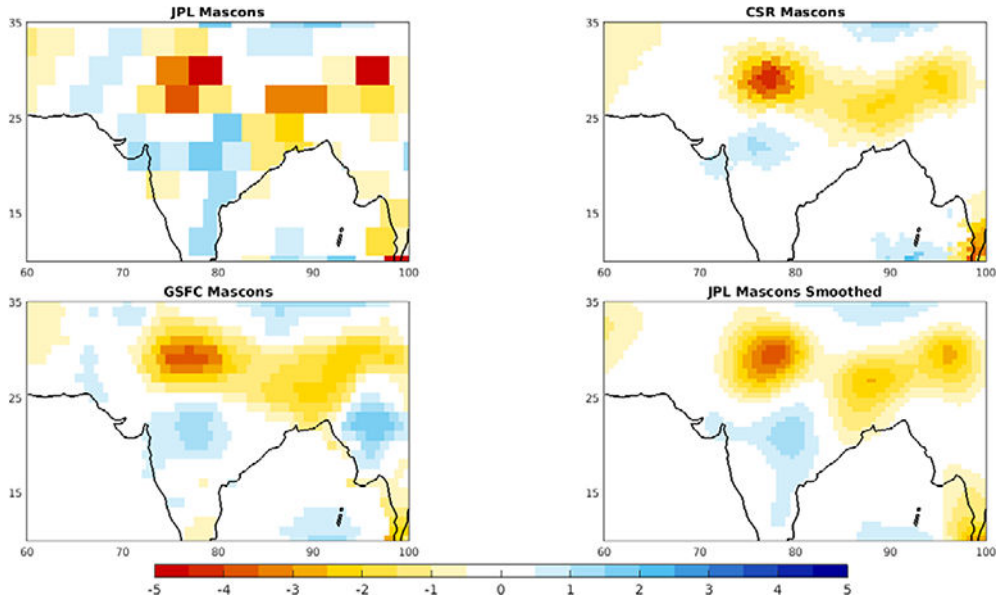

Figure ED9. Comparison of TWS trends (cm/yr) over India (January 2003 - March 2016) from three GRACE mascon solutions.

NASA Author Manuscript

NASA Author Manuscript

NASA Author Manuscript

JPL-M 3° (panel a), CSR-M 1° (b), GSFC-M 1° (c), and JPL-M smoothed with a 200 km radius Gaussian filter and plotted at 1° (d). Notice the similarity between the latter three trend maps, whose regional trend amplitudes have all been dampened by smoothing.

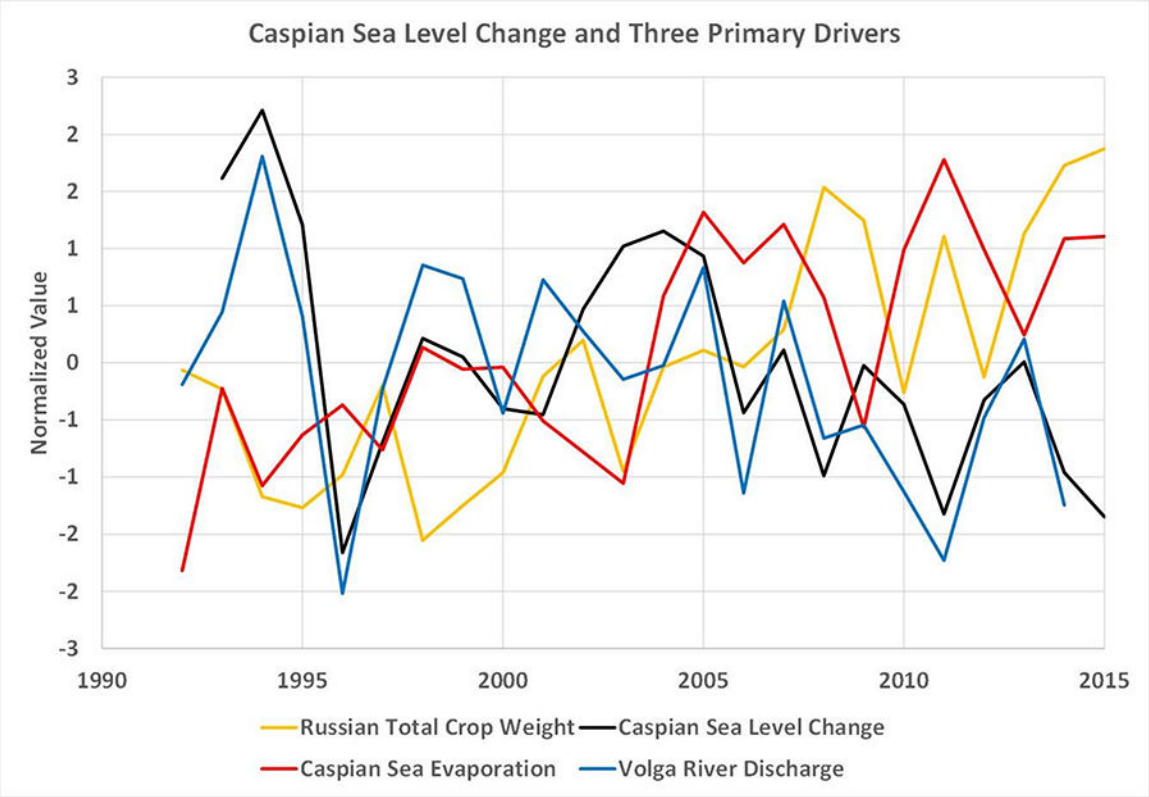

Figure ED10. Comparison of normalized anomalies of Caspian Sea level changes and three primary drivers.

Normalized anomalies of (1) changes in annual mean Caspian Sea level, (2) Volga River discharge, (3) Russian total crop weight, and (4) Caspian Sea evaporation. Precipitation (Figure ED2) is the other primary driver. Sea level change is positively correlated with Volga River discharge is and negatively correlated with Russian crop weight and evaporation.

Acknowledgements

We thank the German Space Operations Center of the German Aerospace Center (DLR) for providing continuously and nearly 100% of the raw telemetry data of the twin GRACE satellites. Landsat is an interagency program managed by NASA and the U.S. Geological Survey. Lake products courtesy of the USDA/NASA G-REALM program at http://www.pecad.fas.usda.gov/cropexplorer/global_reservoir/. Valentina Khan of the Hydrometeorological Research Center of the Russian Federation assisted with the Volga River discharge analysis. Graphics were produced by Amy K. Moran, Global Science & Technology, Inc. This research was funded by NASA's GRACE Science Team and NASA's Energy and Water Cycle Study (NEWS) Team; the University of California Office of the President, Multicampus Research Programs and Initiatives; the NASA Earth and Space Science Fellowship program; the Jet Propulsion Laboratory; and the Ministry of Science and Technology, Taiwan. Portions of this research were conducted at the Jet Propulsion Laboratory, which is operated for NASA under contract with the California Institute of Technology. We also thank two anonymous reviewers for helping to improve the quality of the manuscript.

NASA Author Manuscript NASA Author Manuscript NASA Author Manuscript

References

1. Changnon SA Detecting drought conditions in Illinois. Circular 169 (Illinois State Water Survey, 1987).
2. Rodell M , & Famiglietti JS An analysis of terrestrial water storage variations in Illinois with implications for the Gravity Recovery and Climate Experiment (GRACE). Wat. Resour. Res 37, 1327–1340, doi:10.1029/2000WR900306 (2001).
3. Getirana A , Kumar S , Girotto M , & Rodell M Rivers and floodplains as key components of global terrestrial water storage variability. Geophys. Res. Lett 44, 10359–10368, doi: 10.1002/2017GL074684 (2017).
4. Luthcke SB et al. Antarctica, Greenland and Gulf of Alaska land ice evolution from an iterated GRACE global mascon solution. J. Glac 59, 613–631, doi:10.3189/2013JoG12J147 (2013).
5. Velicogna I , Sutterley TC , & van den Broeke MR Regional acceleration in ice mass loss from Greenland and Antarctica using GRACE time-variable gravity data. Geophys. Res. Lett 41, 8130–8137, doi:10.1002/2014GL061052 (2014).
6. Wada Y , van Beek LPH , & Bierkens MFP Nonsustainable groundwater sustaining irrigation: A global assessment. Water Resour. Res 48, W00L06, doi: 10.1029/2011WR010562 (2012).
7. Konikow LF Contribution of global groundwater depletion since 1900 to sea-level rise. Geophys. Res. Lett 38, L17401, doi: 10.1029/2011GL048604 (2011).
8. Van Dijk AIJM , Renzullo LJ , Wada Y , & Tregoning P A global water cycle reanalysis (2003–2012) merging satellite gravimetry and altimetry observations with a hydrological multi-model ensemble. Hydrol. Earth Syst. Sci, 18, 2955–2973, doi: 10.5194/hess-18-2955-2014 (2014).
9. Zektser IS & Everett LG Groundwater Resources of the World and Their Use. http://unesdoc.unesco.org/images/0013/001344/134433e.pdf (UNESCO, 2004).
10. Siebert S et al. Groundwater use for irrigation - a global inventory. Hydrol. Earth Syst. Sci 14, 1863–1880, doi:10.5194/hess-14-1863-2010 (2010).
11. Vorosmarty CJ et al. Global threats to human water security and river biodiversity. Nature 467, 555–561, doi:10.1038/nature09440 (2010).20882010
12. Syed TH , Famiglietti JS , Chambers DP , Willis JK , & Hilburn K Satellite-based global-ocean mass balance estimates of interannual variability and emerging trends in continental freshwater discharge. Proceedings of the National Academy of Sciences 107, 17916–17921, doi: 10.1073/pnas.1003292107 (2010).
13. Rodell M et al. The observed state of the water cycle in the early 21st century.J. Climate 28, 8289–8318, doi:10.1175/JCLI-D-14-00555.1 (2015).
14. Famiglietti JS et al. Satellites provide the big picture. Science 349, 684–685, doi: 10.1126/science.aac9238 (2015).26273037
15. Tapley BD , Bettadpur S , Ries JC , Thompson PF , & Watkins MM GRACE measurements of mass variability in the Earth system. Science 305, 503–505, doi: 10.1126/science.1099192 (2004). 15273390
16. Wahr J , Molenaar M , & Bryan F Time variability of the Earth's gravity field: Hydrological and oceanic effects and their possible detection using GRACE. J. Geophys. Res. Solid Earth, 103, 30205–30229, doi:10.1029/98JB02844 (1998).
17. Rodell M , & Famiglietti JS Detectability of variations in continental water storage from satellite observations of the time dependent gravity field. Water Resources Res, 35, 2705–2723, doi: 10.1029/1999WR900141 (1999).
18. Swenson S , Yeh PJF , Wahr J , & Famiglietti J A comparison of terrestrial water storage variations from GRACE with in situ measurements from Illinois. Geophys. Res. Lett 33, L16401, doi: 10.1029/2006GL026962 (2006).
19. Cazenave A , & Chen J Time-variable gravity from space and present-day mass redistribution in the Earth system. Earth and Planetary Science Letters, 298, 263–274, doi:10.1016/j.epsl.2010.07.035 (2010).
20. Rowlands DD et al. Resolving mass flux at high spatial and temporal resolution using GRACE intersatellite measurements. Geophys. Res. Lett, 32, L04310, doi: 10.1029/2004GL021908 (2005)

NASA Author Manuscript NASA Author Manuscript NASA Author Manuscript

21. Watkins MM , Wiese DN , Yuan DN , Boening C & Landerer FW Improved methods for observing Earth's time variable mass distribution with GRACE using spherical cap mascons. J. Geophys. Res. Solid Earth 120, 2648–2671, doi: 10.1002/2014JB011547 (2015).
22. Adler R et al. The New Version 2.3 of the Global Precipitation Climatology Project (GPCP) Monthly Analysis Product. http://eagle1.umd.edu/GPCP_ICDR/GPCP_Monthly.html (2016).
23. Salmon JM , Friedl MA , Frolking S , Wisser D , & Douglas EM Global rain-fed, irrigated, and paddy croplands: A new high resolution map derived from remote sensing, crop inventories and climate data. Int. J. Applied Earth Observation and Geoinformation 38, 321–334, doi: 10.1016/jjag.2015.01.014 (2015).
24. Birkett C , Reynolds C , Beckley B , & Doorn B From research to operations: the USDA global reservoir and lake monitor In Coastal altimetry (eds Vignudelli S , Kostianoy AG , Cipollini P , & Benveniste J) 19–50 (Springer, 2011).
25. IPCC Annex I: Atlas of Global and Regional Climate Projections (eds van Oldenborgh GJ et al.) in *Climate Change 2013*: The Physical Science Basis. (eds Stocker TF et al.) 1311–1394 (IPCC, Cambridge Univ. Press, 2013).
26. Tamisiea ME , Leuliette EW , Davis JL , & Mitrovica JX Constraining hydrological and cryospheric mass flux in southeastern Alaska using space-based gravity measurements. Geophys. Res. Lett, 32, L20501, doi:10.1029/2005GL023961 (2005).
27. Gardner AS et al. Sharply increased mass loss from glaciers and ice caps in the Canadian Arctic Archipelago. Nature 473, 357–360, doi:10.1038/nature10089 (2011).21508960
28. Boening C , Lebsock M ,Landerer F , & Stephens G Snowfall-driven mass change on the East Antarctic ice sheet. Geophys. Res. Lett 39, L21501, doi: 10.1029/2012GL053316 (2012).
29. Schlegel N-J et al. Application of GRACE to the assessment of model-based estimates of monthly Greenland Ice Sheet mass balance (2003–2012). The Cryosphere, 10, 1965–1989, doi: 10.5194/tc-10-1965-2016 (2016).
30. MacGregor JA et al. Holocene deceleration of the Greenland Ice Sheet. Science 351, 590–593, doi: 10.1126/science.aab1702 (2016).26912699
31. Reager JT et al. A decade of sea level rise slowed by climate-driven hydrology. Science 351, 699–703, doi: 10.1126/science.aad8386 (2016).26912856
32. Landerer FW , Dickey JO , & Güntner A Terrestrial water budget of the Eurasian pan-Arctic from GRACE satellite measurements during 2003–2009. J. Geophys. Res. Atmospheres 115, D23, doi: 10.1029/2010JD014584 (2010).
33. Famiglietti JS The global groundwater crisis. Nature Climate Change, 4, 945–948, doi: 10.1038/nclimate2425 (2014).
34. Gleeson T , Wada Y , Bierkens MF , & van Beek LP Water balance of global aquifers revealed by groundwater footprint. Nature 488, 197–200, doi:10.1038/nature11295 (2012).22874965
35. Richey AS et al. Uncertainty in global groundwater storage estimates in a total groundwater stress framework. Water Resour. Res, 51, 5198–5216, doi: 10.1002/2015WR017351 (2015).26900184
36. Döll P , Schmied HM , Schuh C , Portmann FT , & Eicker A Global-scale assessment of groundwater depletion and related groundwater abstractions: Combining hydrological modeling with information from well observations and GRACE satellites. Water Resour. Res 50, 5698–5720, doi:10.1002/2014WR015595 (2014).
37. Long D et al. Global analysis of spatiotemporal variability in merged total water storage changes using multiple GRACE products and global hydrological models. Remote Sensing of Environment 192, 198–216, doi:10.1016/j.rse.2017.02.011 (2017).
38. Dalin C , Wada Y , Kastner T , & Puma MJ Groundwater depletion embedded in international food trade. Nature 543, 700–704, doi:10.1038/nature21403 (2017).28358074
39. Phillips T , Nerem R , Fox-Kemper B , Famiglietti J , & Rajagopalan B The influence of ENSO on global terrestrial water storage using GRACE, Geophys. Res. Lett 39, L16705, doi: 10.1029/2012GL052495 (2012).
40. Humphrey V , Gudmundsson L , & Seneviratne SI Assessing global water storage variability from GRACE: Trends, seasonal cycle, subseasonal anomalies and extremes. Surveys in Geophysics 37, 357–395, doi:10.1007/s10712-016-9367-1 (2016).27471333

NASA Author Manuscript NASA Author Manuscript NASA Author Manuscript

41. Rodell M , Velicogna I , & Famiglietti JS Satellite-based estimates of groundwater depletion in India. Nature 460, 999–1002, doi:10.1038/nature08238 (2009).19675570
42. Tiwari VM , Wahr J , & Swenson S Dwindling groundwater resources in northern India, from satellite gravity observations. Geophys. Res. Lett 36, L18401, doi:10.1029/2009GL039401 (2009).
43. Panda DK & Wahr J Spatiotemporal evolution of water storage changes in India from the updated GRACE-derived gravity records. Water Resour. Res 52, 135–149, doi:10.1002/2015WR017797 (2016).
44. Zarfl C , Lumsdon AE , Berlekamp J , Tydecks L , & Tockner K A global boom in hydropower dam construction. Aquatic Sciences 77, 161–170, doi:10.1007/s00027-014-0377-0 (2015).
45. Wang X , de Linage C , Famiglietti J , & Zender CS Gravity Recovery and Climate Experiment (GRACE) detection of water storage changes in the Three Gorges Reservoir of China and comparison with in situ measurements. Water Resour. Res 47, W12502, doi: 10.1029/2011WR010534 (2011).
46. Chao BF , Wu YH , & Li YS Impact of artificial reservoir water impoundment on global sea level. Science, 320, 212–214, doi:10.1126/science.1154580 (2008).18339903
47. Zhang G , Xie H , Kang S , Yi D , & Ackley SF Monitoring lake level changes on the Tibetan Plateau using ICESat altimetry data (2003–2009). Remote Sensing of Environment 115, 1733–1742, doi:10.1016/j.rse.2011.03.005 (2011).
48. Zhang TY & Jin SG Estimate of glacial isostatic adjustment uplift rate in the Tibetan Plateau from GRACE and GIA models. J. Geodynamics, 72, 59–66, doi: 10.1016/j.jog.2013.05.002 (2013).
49. Jacob T , Wahr J , Pfeffer WT , & Swenson S Recent contributions of glaciers and ice caps to sea level rise. Nature 482, 514–518, doi:10.1038/nature10847 (2012).22318519
50. Guo M , Wu W , Zhou X , Chen Y & Li J Investigation of the dramatic changes in lake level of the Bosten Lake in northwestern China. Theor. Appl. Climatol 119, 341–351, doi:10.1007/s00704-014-1126-y (2015).
51. Stone R For China and Kazakhstan, no meeting of the minds on water. Science 337, 405–407, doi: 10.1126/science.337.6093.405 (2012).22837504
52. Hao Y , Zhu Y , Zhao Y , Wang W , Du X & Yeh TCJ The role of climate and human influences in the dry-up of the Jinci Springs, China. J. Am. Water Resour. Assoc 45, 1228–1237, doi:10.1111/j.1752-1688.2009.00356.x (2009).
53. Shamsudduha M , Taylor RG , & Longuevergne L Monitoring groundwater storage changes in the highly seasonal humid tropics: Validation of GRACE measurements in the Bengal Basin. Water Resour. Res 48, W02508, doi:10.1029/2011WR010993 (2012).
54. Voss KA et al. Groundwater depletion in the Middle East from GRACE with implications for transboundary water management in the Tigris-Euphrates-Western Iran region. Water Resour. Res 49, 904–914, doi:10.1002/wrcr.20078 (2013).23658469
55. Sultan M , Ahmed M , Wahr J , Yan E , & Emil M in Remote Sensing of the Terrestrial Water Cycle (eds Lakshmi V *et al.),* 349–366 (John Wiley & Sons, Inc, Hoboken, NJ 2014).
56. Joodaki G , Wahr J , & Swenson S Estimating the human contribution to groundwater depletion in the Middle East, from GRACE data, land surface models, and well observations. Water Resour. Res 50, 2679–2692, doi:10.1002/2013WR014633 (2014).
57. USDA Foreign Agricultural Service. Saudi Arabia Grain and Feed Annual, Global Agricultural Information Network Report number SA1602, http://gain.fas.usda.gov/Recent%20GAIN%20Publications/Grain%20and%20Feed%2 0Annual_Riyadh_Saudi%20Arabia_3-14-2016.pdf (2016).
58. Becker RH The stalled recovery of the Iraqi marshes. Remote Sensing 6, 1260– 1274, doi:10.3390/rs6021260 (2014).
59. Chao N , Luo Z , Wang Z , & Jin T Retrieving Groundwater Depletion and Drought in the Tigris-Euphrates Basin Between 2003 and 2015. Groundwater, doi:10.1111/gwat.12611 (2017).
60. Zmijewski K , & Becker R Estimating the effects of anthropogenic modification on water balance in the Aral Sea watershed using GRACE: 2003–12. Earth Interactions 18, 1–16, doi: 10.1175/2013EI000537.1 (2014).

NASA Author Manuscript NASA Author Manuscript NASA Author Manuscript

61. Chen JL , Pekker T , Wilson CR , Tapley BD , Kostianoy AG , Cretaux J-F , & Safarov ES Long-term Caspian Sea level change. Geophys. Res. Lett 44, 6993– 7001, doi:10.1002/2017GL073958 (2017).
62. Han S-C , Sauber J , Luthcke SB , Ji C , & Pollitz SS Implications of postseismic gravity change following the great 2004 Sumatra-Andaman earthquake from the regional harmonic analysis of GRACE intersatellite tracking data. J. Geophys. Res. Solid Earth 113, B11413, doi: 10.1029/2008JB005705 (2008).
63. Han SC , Sauber J , & Riva R Contribution of satellite gravimetry to understanding seismic source processes of the 2011 Tohoku-Oki earthquake. Geophys. Res. Lett 38, L24312, doi: 10.1029/2011GL049975 (2011).
64. Peltier WR ., Argus DF , & Drummond R Space geodesy constrains ice age terminal deglaciation: The global ICE-6GC (VM5a) model. J. Geophys. Res. Solid Earth 120, 450–487, doi: 10.1002/2014JB011176 (2015).
65. Peltier WR , Argus DF & Drummond R Comment on the paper by Purcell et al (2016) entitled “An Assessment of the ICE-6G_C (VM5a) glacial isostatic adjustment model. J. Geophys. Res. Solid Earth 122, doi:10.1002/2016JB013844 (2017).
66. Forman BA , Reichle RH , & Rodell M , Assimilation of terrestrial water storage from GRACE in a snow-dominated basin. Water Resour. Res 48, W01507, doi:10.1029/2011WR011239 (2012).
67. Bouchard F et al. Vulnerability of shallow subarctic lakes to evaporate and desiccate when snowmelt runoff is low. Geophys. Res. Lett 40, 6112–6117, doi:10.1002/2013GL058635 (2013).
68. Reager JT et al. Assimilation of GRACE terrestrial water storage observations into a land surface model for the assessment of regional flood potential. Remote Sensing 7, 14663–14679, doi: 10.3390/rs71114663 (2015).
69. Famiglietti JS et al. Satellites measure recent rates of groundwater depletion in California’s Central Valley. Geophys. Res. Lett 38, L03403, doi:10.1029/2010GL046442 (2011).
70. Scanlon BR , et al. Groundwater depletion and sustainability of irrigation in the US High Plains and Central Valley. PNAS 109, 9320–9325, doi:10.1073/pnas.1200311109 (2012).22645352
71. Faunt CC , Sneed M , Traum J & Brandt JT Water availability and land subsidence in the Central Valley, California, USA. Hydrogeology Journal 24, 675– 684, doi:10.1007/s10040-015-1339-x (2016).
72. Belmecheri S , Babst F , Wahl ER , Stahle DW , & Trouet V Multi-century evaluation of Sierra Nevada snowpack. Nature Climate Change, 6, 2–3, doi: 10.1038/nclimate2809 (2016).
73. Fernando DN et al. What caused the spring intensification and winter demise of the 2011 drought over Texas?. Climate Dynamics 47, 3077–3090, doi:10.1007/s00382-016-3014-x (2016).
74. Haacker EM , Kendall AD , & Hyndman DW Water level declines in the high plains aquifer: Predevelopment to resource senescence. Groundwater 54, 231–242, doi: 10.1111/gwat.12350 (2016).
75. Willis MJ , Melkonian AK , Pritchard ME , & Ramage JM Ice loss rates at the Northern Patagonian Icefield derived using a decade of satellite remote sensing. Remote Sensing of Environment 117, 184–198, doi:10.1016/j.rse.2011.09.017 (2012).
76. Chen JL , Wilson CR , Tapley BD , Blankenship DD , & Ivins ER Patagonia icefield melting observed by gravity recovery and climate experiment (GRACE). Geophys. Res. Lett 34, L22501, doi:10.1029/2007GL031871 (2007).
77. Han SC , Sauber J , & Luthcke S Regional gravity decrease after the 2010 Maule (Chile) earthquake indicates large-scale mass redistribution. Geophys. Res. Lett 37, L23307, doi: 10.1029/2010GL045449 (2010).
78. Chen JL , Wilson CR , & Tapley BD The 2009 exceptional Amazon flood and interannual terrestrial water storage change observed by GRACE. Water Resour Res 46, W12526, doi: 10.1029/2010WR009383 (2010).
79. Thomas AC , Reager JT , Famiglietti JS , & Rodell M A GRACE-based water storage deficit approach for hydrological drought characterization. Geophys. Res. Lett 41, 1537–1545, doi: 10.1002/2014GL059323 (2014).
80. Getirana AC Extreme water deficit in Brazil detected from space. J. Hydrometeorol 17, 591–599, doi:10.1175/JHM-D-15-0096.1 (2015).

NASA Author Manuscript NASA Author Manuscript NASA Author Manuscript

81. Gaughan AE & Waylen PR Spatial and temporal precipitation variability in the Okavango-Kwando-Zambezi catchment, southern Africa. J. Arid Environments 82, 19–30, doi:10.1016/j.jaridenv.2012.02.007 (2012).
82. Andersen OB , et al. Terrestrial water storage from GRACE and satellite altimetry in the Okavango Delta (Botswana) Gravity, Geoid and Earth Observation, International Association of Geodesy Symposia Vol. 135 (ed. Mertikas S) 521–526 (Springer, 2010).
83. Swenson S , & Wahr J Monitoring the water balance of Lake Victoria, East Africa, from space. J. Hydrology 370, 163–176, doi:10.1016/j.jhydrol.2009.03.008 (2009).
84. Ahmed M , Sultan M , Wahr J , & Yan E The use of GRACE data to monitor natural and anthropogenic induced variations in water availability across Africa. Earth-Sci. Rev 136, 289–300, doi:10.1016/j.earscirev.2014.05.009 (2014).
85. Ndehedehe CE , Awange JL , Kuhn M , Agutu NO , & Fukuda Y Climate teleconnections influence on West Africa's terrestrial water storage. Hydrological Proc. 31, 3206–3224, doi:10.1002/hyp.11237 (2017).
86. Crowley JW , Mitrovica JX , Bailey RC , Tamisiea ME , & Davis JL Land water storage within the Congo Basin inferred from GRACE satellite gravity data. Geophys. Res. Lett 33, L19402, doi:10.1029/2006GL027070 (2006).
87. Ramillien G , Frappart F , & Seoane L Application of the regional water mass variations from GRACE satellite gravimetry to large-scale water management in Africa. Remote Sensing 6), 7379–7405, doi:10.3390/rs6087379 (2014).
88. Van Dijk A et al. The Millennium Drought in southeast Australia (2001–2009): Natural and human causes and implications for water resources, ecosystems, economy, and society. Water Resources Res. 49, 1040–1057, doi:10.1002/wrcr.20123 (2013).
89. Boening C , Willis JK , Landerer FW , Nerem RS , & Fasullo J The 2011 La Nina: So strong, the oceans fell. Geophys. Res. Lett 39, L19602, doi:10.1029/2012GL053055 (2012).
90. Munier S ,Becker M , Maisongrande P , &Cazenave A Using GRACE to detect Groundwater Storage variations: the cases of Canning Basin and Guarani aquifer system. Int. Water Tech. J 2, 2–13 (2012).
91. Jaramillo F , & Destouni G Local flow regulation and irrigation raise global human water consumption and footprint. Science 350, 1248–1251, doi:10.1126/science.aad1010 (2015). 26785489
92. Fietelson E The four Eras of Israeli water policy Water policy in Israel: Context, Issues and Options (ed. Becker N) 15–32 (Springer, 2013).
93. Bhanja SN et al.Groundwater rejuvenation in parts of India influenced by water734 policy change implementation. Scientific Reports 7, 7453, doi:10.1038/s41598-017-07058-2 (2017).28785088
94. Eicker A , Forootan E , Springer A , Longuevergne L , & Kusche J Does GRACE see the terrestrial water cycle "intensifying"?. J. Geophys. Res. Atmos 121, 733–745, doi:10.1002/2015JD023808 (2016).
95. Kusche J , Eicker A , Forootan E , Springer A , & Longuevergne L Mapping probabilities of extreme continental water storage changes from space gravimetry. Geophys. Res. Lett 43, 8026–8034, doi:10.1002/2016GL069538 (2016).
96. Green TR et al. Beneath the surface of global change: Impacts of climate change on groundwater. J.Hydrology 405, 532–560, doi:10.1016/j.jhydrol.2011.05.002 (2011).
97. Taylor RG et al. Ground water and climate change. Nature Climate Change 3, 322– 329, doi:10.1038/nclimate1744 (2013).
98. Swenson SC , & Milly PCD Climate model biases in seasonality of continental water storage revealed by satellite gravimetry. Water Resour. Res 42, W03201, doi:10.1029/2005WR004628 (2006).
99. McCabe MF et al. The future of Earth observation in hydrology. Hydrology and Earth System Science 21, 3879–3914, doi:10.5194/hess-21-3879-2017 (2017).
100. Flechtner F et al. What can be expected from the GRACE-FO Laser Ranging Interferometer for Earth Science applications?. Surveys in Geophysics 37, 453–470, doi:10.1007/s10712-015-9338-y (2016).

NASA Author Manuscript NASA Author Manuscript NASA Author Manuscript

101. Landerer FW , & Swenson SC (2012). Accuracy of scaled GRACE terrestrial water storage estimates. Water Resour. Res 48, W04531, doi: 10.1029/2011WR011453 (2012).
102. Dahle C , et al. GFZ RL05: an improved time-series of monthly GRACE gravity field solutions Observation of the System Earth from Space-CHAMP, GRACE, GOCE and Future Missions (eds. Flechtner F , Sneeuw N , & Schuh WD) 29–39 (Springer, 2014).
103. Mayer-Gürr T , et al. ITSG-Grace2016 -Monthly and Daily Gravity Field Solutions from GRACE. GFZ Data Services 10.5880/icgem.2016.007 (2016).
104. Bruinsma S , Lemoine J-M , Biancale R , & Vales N CNES/GRGS 10-day gravity field models (release 02) and their evaluation. Adv. Space Res, 45, 587–601, doi:10.1016/j.asr.2009.10.012 (2010).
105. Kurtenbach E , et al. Improved daily GRACE gravity field solutions using a Kalman smoother. J. Geodynamics, 59–60, 39–48 (2012).
106. Liu X , et al. DEOS Mass Transport model (DMT-1) based on GRACE satellite data: methodology and validation. Geophys. J. Int, 181, 769–788, doi: 10.1111/j.1365-246X. 2010.04533.x (2010).
107. Swenson S , & Wahr J Post-processing removal of correlated errors in GRACE data. Geophys. Res. Lett 33, L08402, doi:10.1029/2005GL025285 (2006).
108. Andrews SB , Moore P , & King MA Mass change from GRACE: a simulated comparison of Level-1B analysis techniques. Geophys. J. Int, 200, 503– 518, doi:10.1093/gji/ggu402 (2011).
109. Save H , Bettadpur S , & Tapley BD High resolution CSR GRACE RL05 mascons. J. Geophs. Res. Solid Earth, 121, 7547–7569, doi:10.1002/2016JB013007 (2016).
110. Landerer FW , Wiese DN , Bentel K , Boening C , & Watkins MM North Atlantic meridional overturning circulation variations from GRACE ocean bottom pressure anomalies. Geophys. Res. Lett, 42, 8114–8121, doi:10.1002/2015GL065730 (2015).
111. Wiese DN , Yuan D-N , Boening C , Landerer FW , & Watkins MM JPL GRACE Mascon Ocean, Ice, and Hydrology Equivalent Water Height RL05M.1 CRI Filtered Version 2. PO.DAAC, CA, USA. doi:10.5067/TEMSC-2LCR5 (2016).
112. Wiese DN , Landerer FW , & Watkins MM Quantifying and reducing leakage errors in the JPL RL05M GRACE mascon solution. Water Resour. Res 52, 7490–7502, doi: 10.1002/2016WR019344 (2016).
113. Cheng M & Tapley BD Variations in the Earth's oblateness during the past 28 years. J. Geophys. Res 109, B09402 (2004).
114. Swenson S , Chambers D , & Wahr J Estimating geocenter variations from a combination of GRACE and ocean model output. J. Geophys. Res 113, B08410, doi: 10.1029/2004JB003028 (2008).
115. Ivins ER et al. Antarctic contribution to sea level rise observed by GRACE with improved GIA correction, J. Geophys. Res 118, 3126–3141, doi: 10.1002/jgrb.50208 (2013).
116. Shepherd A , et al. A reconciled estimate of ice-sheet mass balance. Science, 338, 1183–1189, doi:10.1126/science.1228102 (2012).23197528
117. Wahr J , Nerem RS , & Bettadpur SV The pole tide and its effect on GRACE time variable gravity measurements: Implications for estimates of surface mass variations. J. Geophys. Res. Solid Earth 120, 4597–4615, doi:10.1002/2015JB011986 (2015).
118. Fagiolini E , Flechtner F , Horwath M , & Dobslaw H Correction of inconsistencies in ECMWF's operational analysis data during de-aliasing of GRACE gravity models. Geophy. J. Int 202, 2150–2158, doi:10.1093/gji/ggv276 (2015).
119. Scanlon BR et al. Global evaluation of new GRACE mascon products for hydrologic applications. Water Resourc. Res, 52, 9412– 9429 10.1002/2016WR019494 (2016).
120. Chen JL , Wilson CR , Tapley BD , Save H , & Cretaux J-F Long-term and seasonal Caspian Sea level change from satellite gravity and altimeter measurements. J. Geophys. Res. Solid Earth, 122, 2274–2290, doi:10.1002/2016JB013595 (2017).
121. A G , Wahr J & Zhong S Computations of the viscoelastic response of a 3-D compressible Earth to surface loading: An application to Glacial Isostatic Adjustment in Antarctica and Canada. Geophys. J. Int 192, 557–572, doi:10.1093/gji/ggs030 (2013).

NASA Author Manuscript NASA Author Manuscript NASA Author Manuscript

122. Paulson A , Zhong S , & Wahr J Inference of mantle viscosity from GRACE and relative sea level data. Geophys. J. Int 171, 497–508, doi:10.1111/j.1365-246X.2007.03556.x (2007).
123. Purcell A , Tregoning P , & Dehecq A An assessment of the *ICE6G_C(VM5a)* glacial isostatic adjustment model. J. Geophys. Res. Solid Earth 121, 3939–3950, doi:10.1002/2015JB012742 (2016).
124. Purcell A , Tregoning P , &Dehecq A Reply to comment by Peltier WR , Argus DF , and Drummond R on “An assessment of the ICE6G C (VM5a) glacial isostatic adjustment model. J. Geophys. Res. Solid Earth 122, doi:10.1002/2017JB014930 (2017).
125. Landerer FW , and Swenson SC Accuracy of scaled GRACE terrestrial water storage estimates. Water Resour. Res, 48, W04531, doi:10.1029/2011WR011453 (2012).
126. Rodell M , et al. The global land data assimilation system. Bull. Amer. Meteorol. Soc 85, 381–394, doi:10.1175/BAMS-85-3-381 (2004).
127. Cretaux J-F , et al. SOLS: A lake database to monitor in the near real time water level and storage variations from remote sensing data. Adv. Space Res 47, 1497–1507, doi:10.1016/j.asr.2011.01.004 (2011).
128. Avakyan AB Volga-Kama cascade reservoirs and their optimal use. Lakes & Reservoirs Research & Management 3, 113–121, doi:10.1111/j.1440-1770.1998.tb00038.x (1998).
129. OECD, Crop production (indicator). doi:10.1787/49a4e677-en. Accessed online at https://data.oecd.org/agroutput/crop-production.htm (2017).
130. Gelaro R , et al. The modern-era retrospective analysis for research and applications, version 2 (MERRA-2). J. Clim 30, 5419–5454, doi:10.1175/JCLI-D-16-0758.1 (2017).
131. Farinotti D et al. Substantial glacier mass loss in the Tien Shan over the past 50 years. Nature Geoscience 8, 716–722, doi:10.1038/ngeo2513 (2015).
132. Gardner A et al. A reconciled estimate of glacier contributions to sea level rise: 2003 to 2009. Science 340, 852–857, doi: 10.1126/science.1234532 (2013).23687045
133. Mou D & Li Z A spatial analysis of China’s coal flow. Energy Policy 48, 358– 368, doi:10.1016/j.enpol.2012.05.034 (2012).
134. Feng W et al. Evaluation of groundwater depletion in North China using the Gravity Recovery and Climate Experiment (GRACE) data and ground-based measurements. Water Resour. Res 49, 2110–2118, doi:10.1002/wrcr.20192 (2013).
135. Moiwo JP , Tao F , & Lu W Analysis of satellite-based and in situ hydro1129 climatic data depicts water storage depletion in North China Region. Hydrological Proc. 27, 1011–1020, doi:10.1002/hyp.9276 (2013).
136. Tang Q , Zhang X , & Tang Y Anthropogenic impacts on mass change in North China. Geophys. Res. Lett 403924–3928, doi:10.1002/grl.50790 (2013).
137. Ebead B , Ahmed M , Niu Z , & Huang N Quantifying the anthropogenic impact on groundwater resources of North China using Gravity Recovery and Climate Experiment data and land surface models. J.Applied Remote Sensing 11, 026029–026029, doi:10.1117/1.JRS.11.026029 (2017).

NASA Author Manuscript

NASA Author Manuscript

NASA Author Manuscript

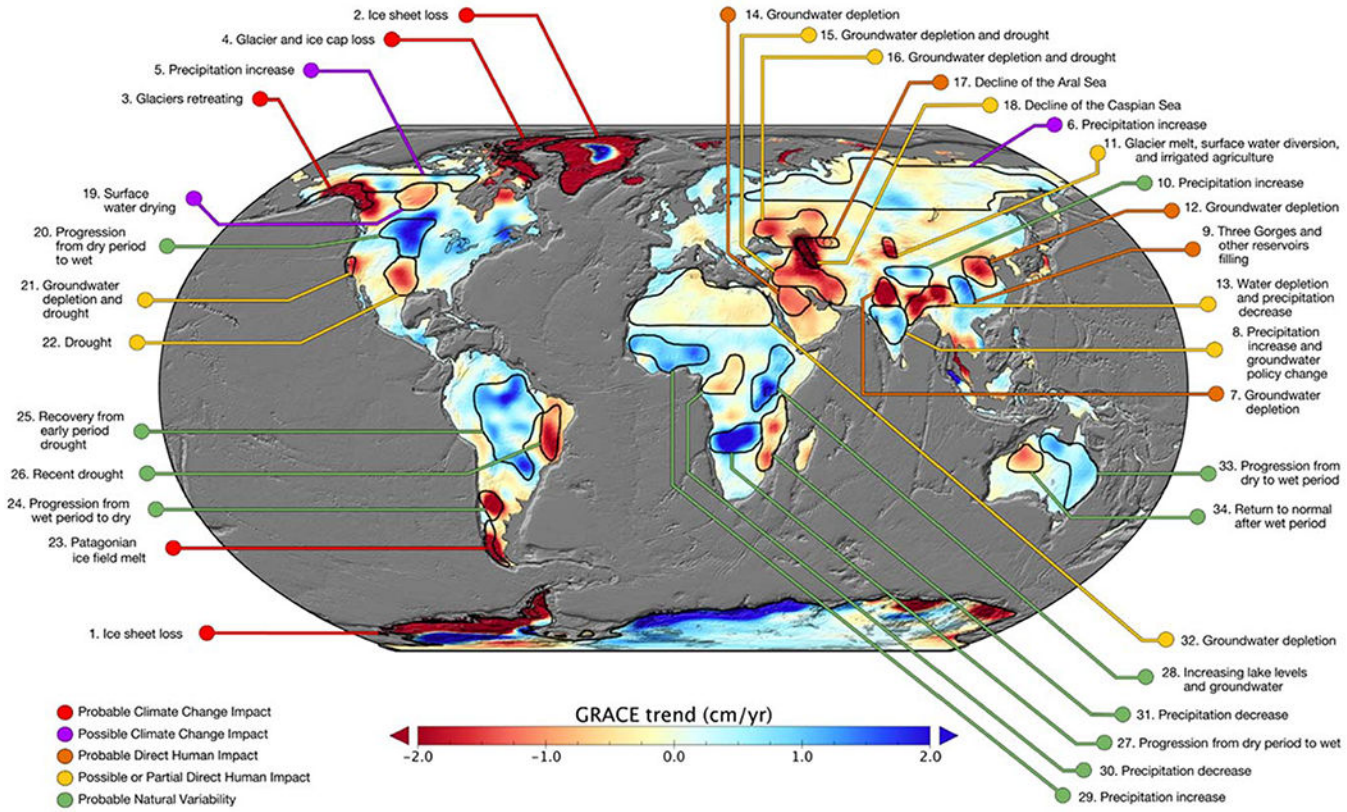

Figure 1. Annotated map of terrestrial water storage trends

. Trends in TWS (cm/yr) based on GRACE observations from April 2002 to March 2016. The cause of the trend in each outlined study region is briefly explained and color coded by category. The trend map was smoothed with a 150 km radius Gaussian filter for the purpose of visualization, however, all calculations were performed at the native 3° resolution of the data product.

NASA Author Manuscript NASA Author Manuscript NASA Author Manuscript

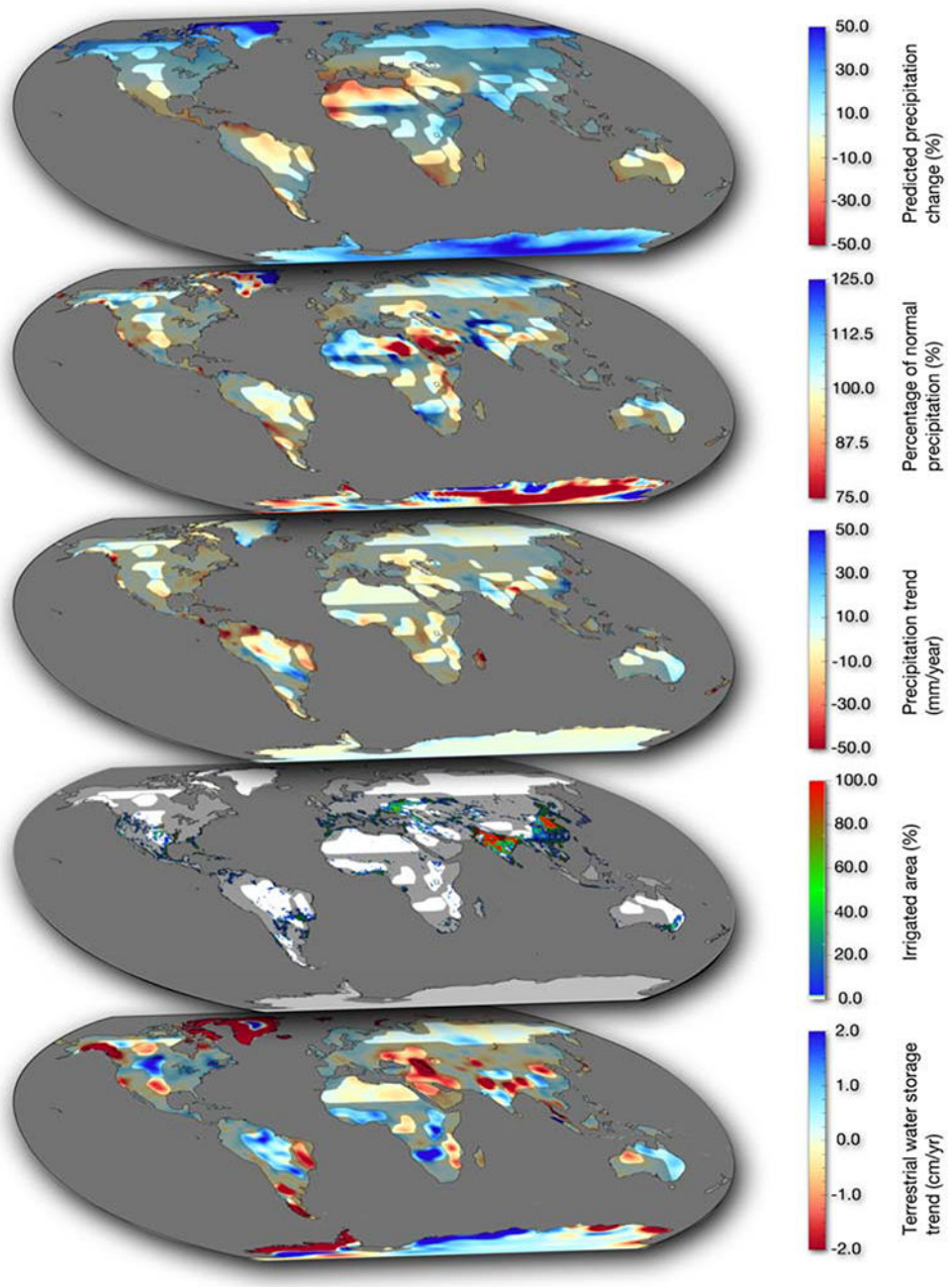

Figure 2. Trends in terrestrial water storage and supporting data maps

.

(Bottom to top) TWS trends (cm/yr); percentage of area equipped for irrigation[23] (%); trend in precipitation[22]; mean annual precipitation (2003–2015) as a percentage of the long term mean[22]; IPCC predicted change in precipitation[25]. Areas outside of the study regions are shaded.

NASA Author Manuscript

NASA Author Manuscript

NASA Author Manuscript

Table 1.

TWS trends and supporting information. Location, area, GRACE terrestrial water storage trend (April 2002 - March 2016) and uncertainty, coefficient of determination (r^2) of the fitted linear trend, percentage of the area equipped for irrigation[23], trend in precipitation[22] (January 2002 to March 2016) after removing the seasonal cycle, annual mean precipitation (2003–2015) as a percentage of the long term (1979–2015) annual mean[22], and median predicted change in precipitation between 1986–2005 and 2081–2100 in the IPCC high end greenhouse gas emissions scenario[25] for each of the 34 study regions. *The TWS Trend in Region 24 is for April 2002 -February 2010 only.

Region #	Location	Area (km^2)	TWS Trend (Gt/yr)	TWS Trend Errors (Gt/yr)	R^2 of TWS Trend (−)	Irrigated Area (%)	Precipitation Trend (mm/yr)	Precipitation Trend (%/yr)	Precipitation Percentage of Normal (%)	Predicted Precipitation Change (%)
1	Antarctica	12,397,401	−127.6	39.9	0.93	0	0.82	0.40	96.6	30.9
2	Greenland	2,184,307	−279.0	23.2	0.97	0	8.85	2.09	102.7	39.1
3	Gulf Coast of Alaska	716,492	−62.6	8.2	0.93	0	−3.03	−0.25	95.0	21.3
4	Canadian Archipelago	672,413	−74.6	4.1	0.95	0	−5.33	−2.11	94.5	38.3
5	N North America	1,350,129	6.1	5.8	0.52	0	2.35	0.73	105.1	26.9
6	N Eurasia	8,009,175	13.4	9.7	0.10	0	1.65	0.30	104.4	25.1
7	N India	664,169	−19.2	1.1	0.80	54	15.80	2.20	101.0	11.8
8	Central India	1,352,670	9.4	0.6	0.24	51	3.72	0.36	103.7	23.1
9	E Central China	657,375	7.8	1.6	0.78	14	7.33	0.77	99.6	7.9
10	Tibetan Plateau	881,704	7.7	1.4	0.67	0	−1.52	−0.90	104.2	19.7
11	NW China	215,152	−5.5	0.5	0.77	7	1.11	0.57	109.8	15.3
12	N China Plain	876,004	−11.3	1.3	0.63	52	−2.33	−0.37	103.0	19.4
13	E India Region	1,228,839	−23.3	1.9	0.85	25	−9.52	−0.67	96.1	14.7
14	NW Saudi Arabia	841,763	−10.5	1.5	0.92	0	−1.44	−1.31	77.7	−1.4
15	N Middle East	2,189,561	−32.1	1.5	0.84	5	−2.80	−0.90	96.3	−8.5
16	SW Russia Region	1,772,712	−18.1	1.3	0.64	15	−5.83	−0.92	96.8	6.2
17	Aral Sea	52,299	−2.2	0.1	0.76	0	2.71	1.17	111.1	5.9
18	Caspian Sea	377,761	−23.7	4.2	0.76	0	−4.37	−1.14	103.4	2.1
19	Central Canada	802,682	−7.0	6.4	0.73	0	0.69	0.17	102.0	16.9
20	N Great Plains	1,333,598	20.2	4.8	0.79	3	2.26	0.44	102.0	7.0
21	S California	177,996	−4.2	0.4	0.46	18	−8.31	−1.29	89.7	1.2
22	S High Plains and E Texas	1,105,113	−12.2	3.6	0.44	9	−5.71	−0.76	95.2	−2.8
23	Patagonian Ice Fields	461,198	−25.7	5.1	0.89	0	−8.01	−0.76	97.1	−6.9
24	Central Argentina*	530,661	−8.6	1.2	0.77	4	1.87	0.32	94.2	0.7

NASA Author Manuscript

NASA Author Manuscript

NASA Author Manuscript

Region #	Location	Area (km^2)	TWS Trend (Gt/yr)	TWS Trend Errors (Gt/yr)	R^2 of TWS Trend (−)	Irrigated Area (%)	Precipitation Trend (mm/yr)	Precipitation Trend (%/yr)	Precipitation Percentage of Normal (%)	Predicted Precipitation Change (%)
25	Central & W Brazil	5,559,805	51.9	9.4	0.39	1	0.61	0.03	100.2	−5.0
26	E Brazil	1,132,450	−16.7	2.9	0.39	1	−16.97	−1.61	97.7	−5.9
27	Okavango Delta	1,589,692	29.5	3.5	0.55	0	−5.21	−0.61	105.3	−8.7
28	Nile Headwaters	1,824,276	21.9	3.9	0.56	1	−3.53	−0.30	97.7	11.6
29	Tropical W Africa	2,298,134	24.1	2.1	0.67	1	−0.12	−0.01	103.4	−6.3
30	N Congo	1,318,261	−7.2	1.0	0.26	0	−1.55	−0.10	99.1	7.1
31	SE Africa	1,677,719	−12.9	2.3	0.47	0	−3.23	−0.32	95.9	−5.9
32	N Africa	6,664,135	−11.7	2.9	0.45	1	−0.12	−0.19	106.7	−12.9
33	N & E Australia	2,504,494	19.0	2.8	0.32	3	4.30	0.69	104.6	−6.0
34	NW Australia	1,002,367	−8.9	1.2	0.43	0	−0.39	−0.10	99.1	−0.6